UNIVERSITY OF CALIFORNIA
RIVERSIDE

# Air Quality Impact of Distributed Generation of Electricity

A Dissertation submitted in partial satisfaction
of the requirements for the degree of

Doctor of Philosophy

in

Mechanical Engineering

by

Qiguo Jing

December 2011

Dissertation Committee:
Dr. Akula Venkatram, Chairperson
Dr. Marko Princevac
Dr. Guillermo Aguilar

The Dissertation of Qiguo Jing is approved:

_____

_____

_____

Committee Chairperson

University of California, Riverside

ACKNOWLEDGEMENTS

First and foremost I offer my sincerest gratitude to my advisor Professor Akula Venkatram who continuously guided, encouraged and supported me in the course of this study. His attitude, passion, and dedication for research and teaching affect and inspire me in every aspect of my life.

I would like to thank my committee members, Dr. Marko Princevac and Dr. Guillermo Aguilar, for their insightful comments and recommendations on my dissertation. Dr. Marko Princevac and his research group made major contributions in collecting and preparing the data sets which I have been using for my research.

I appreciate my colleagues in the Air Quality and Fire Engineering group at the University of California, Riverside, for their hard work, thoughtful discussion and friendly support: Dr. Wenjun Qian, Dr. Xiangyi Li, Dr. Tao Zhan, Ms. Si Tan, Mr. Nico Schulte, Mr. Sam Pournazeri and Mr. Christian Bartolome. I would also like to thank all my teammates from the Table Tennis Club and all other friends at UCR.

I am so grateful to my wife Hansheng Pan, who has been accompanying me for more than seven years, for her personal support and great patience at all times.

Special thanks go to my parents and parents-in-law for their endless love, support, and encouragement.

My research was supported by the California Energy Commission (Grant # MAQ-07-03).

The text of this dissertation, in part, is a reprint of the material as it appears in Energy Policy (2011) 39, 4999-5007. The co-author Akula Venkatram directed and supervised the research which forms the basis for this dissertation.

ABSTRACT OF THE DISSERTATION

Air Quality Impact of Distributed Generation of Electricity

by

Qiguo Jing

Doctor of Philosophy, Graduate Program in Mechanical Engineering
University of California, Riverside, December 2011
Dr. Akula Venkatram, Chairperson

This dissertation summarizes the results of a five-year investigation of the impact of distributed generation (DG) of electricity on air quality in urban areas. I focused on the impact of power plants with capacities of less than 50 MW, which is typical of DG units in urban areas. These power plants are modeled as buoyant emissions from stacks less than 10 m situated in the midst of urban buildings. Because existing dispersion models are not designed for such sources, the first step of the study involved the evaluation of AERMOD, USEPA's state-of-the art dispersion model, with data collected in a tracer study conducted in the vicinity of a DG unit. The second step of the study consisted of using AERMOD to compare the impact of DG penetration in the South Coast Air Basin of Los Angeles with the impact of replacing DG generation with expansion of current central power plant capacity. The third topic of my investigation is the development and application of a model to examine the impact of non-power plant sources in a large urban area such as Los Angeles. This model can be used to estimate the air quality impact of DG relative to other sources in an urban area.

The first part of this dissertation describes a tracer study conducted in Palm Springs, CA. Concentrations observed during the nighttime experiments are generally higher than those measured during the daytime experiments. They fall off less rapidly with distance than during the daytime. AERMOD provides an adequate description of concentrations associated with the buoyant releases from the DG during the daytime when turbulence is controlled by convection induced by solar heating. However, AERMOD underestimates concentrations during the night when turbulence is generated by wind shear. Also, AERMOD predicts a decrease in concentrations with distance that is much more rapid than the relatively flat observed decrease. I have suggested modifications to AERMOD to improve the agreement between model estimates and observations during the night.

The second part of this dissertation examines the air quality impact of using DG to satisfy future growth in power demand in the South Coast Air Basin of Los Angeles (SoCAB), relative to the impact when the demand is met by expanding current central generation (CG) capacity. The air quality impacts of these two alternate scenarios are quantified in terms of hourly maximum ground-level and annually-averaged primary $NO_x$ concentrations, which are estimated using AERMOD. The shift to DGs has the potential for decreasing maximum hourly impacts of power generation in the vicinity of the DGs. The maximum hourly concentration is reduced from 25 ppb to 6 ppb if DGs rather than CGs are used to generate power. However, the annually-averaged concentrations are likely to be higher than for the scenario in which existing CGs are used to satisfy power demand growth. Future DG penetration will add an annual average of 0.1 ppb to the current basin average, 20 ppb, while expanding existing CGs will add 0.05 ppb.

The third part of my dissertation focused on formulating a model to estimate concentrations of $NO_2$, $NO_x$, and $O_3$ averaged over a spatial scale of the order of a kilometer in a domain extending over tens of kilometers. The model can be used to estimate hourly concentrations of these species over time periods of years. It achieves the required computational efficiency by separating transport and chemistry using the concept of species age. Evaluation with data measured at 21 stations distributed over the Los Angeles air basin indicates that the model provides an adequate description of the spatial and temporal variation of the concentrations of $NO_2$ and $NO_x$. Estimates of maximum hourly $O_3$ concentrations show little bias compared to observations, but the scatter is not small.

List of Contents

List of Figures

List of Tables

# 1. Introduction and Objectives

## 1.1 Problem Area and Approach

Distributed generation (DG) has the potential to meet a significant portion of increased power demand because of the following advantages: 1) reduction in electricity transmission losses because DG units are located in the area they service, 2) flexibility in size tailored to local power demand; 3) increase in efficiency and decrease in emissions by replacing boilers by Combined Heat and Power (CHP) systems. It may serve a single home, neighborhood, or business more efficiently and reliably than a centrally located power plant, and at a lower cost (Allison and Lents 2002). These benefits and the continuing concerns about the power reliability, quality, costs, and evolving technology have all contributed to the use of DG.

Small DG units have the potential of causing air quality problems because they emit pollutants from relatively short stacks, and they are usually located in populated urban neighborhoods. A single DG may have an impact on air quality at scales of tens of meters from the source, while the cumulative impact of several DGs located in an urban area will affect air quality at scales of kilometers from the source. The overall objective of this thesis is to develop methods to estimate the air quality impacts of DG on $NO_x$ and $NO_2$ relative to other sources of $NO_x$ over scales ranging from meters to kilometers.

The air quality impact of DGs can, in principle, be estimated using a combination of a short-range dispersion model, such as AERMOD (AMS/EPA Regulatory Model, Cimorelli et al., 2005) and a long-range transport model such as CMAQ (Community

Multiscale Air Quality, Byun and Ching, 1999). Models such as AERMOD are designed to estimate the air quality impact of isolated sources in a spatially homogenous area. They have not been tested adequately in an urban area, which has a complex spatially varying surface. DG units emit pollutants from relatively short stacks, which can be below the heights of the surrounding buildings. Even though DG exhaust gases are usually hot and thus buoyant, the emitted plumes are affected by buildings. Furthermore, the micrometeorology (Britter and Hanna, 2003) that governs the dispersion of these plumes is a strong function of the complex urban surface. Thus, modeling dispersion at short distances from a DG unit poses major problems. This thesis addresses the solution of some these problems. It also provides an approach to estimating the cumulative air quality impact of several DGs relative to those of central generating stations and other sources in a large urban area.

This thesis applies AERMOD (Cimorelli et al., 2005) to the South Coast Air Basin of Los Angles to examine the relative impact of distributed and centralized generation of electricity on local air quality. Before doing so, this thesis examines the applicability of the current generation of dispersion models such as AERMOD to a DG, which represents a low level buoyant source in an urban area. This thesis also presents a Lagrangian model to estimate background concentrations of $NO_2$, $NO_x$, and $O_3$ associated with other urban sources. These concentrations are averaged over a spatial scale of the order of a kilometer in a domain extending over tens of kilometers. Finally, this thesis compares the impact of emissions from a DG on urban air quality estimated using AERMOD with the impact of

emissions from all other sources predicted by the Lagrangian model. The next section reviews past studies relevant to the research described in this thesis.

## 1.2 Background

### 1.2.1 Vertical Structural of Urban Boundary Layer

The atmospheric boundary layer or the planetary boundary layer (PBL) is the part of the troposphere that is directly influenced by the presence of the earth's surface, and it responds to surface forcing with a timescale of about an hour or less (Stull 1988). The troposphere exchanges momentum, heat, and mass with the ground through the PBL. The turbulence within the PBL is produced by shear stresses associated with gradients in the horizontal wind and vertical motion induced by buoyant air parcels rising from the surface heated by solar radiation.

The urban boundary layer (UBL) is formed when air flows from a rural area to an urban area. The surface roughness increases from rural to urban areas, and the urban surface temperature is usually higher than the rural temperature. Figure 1-1 shows the vertical structures of the urban and rural boundary layers, which is adapted from Grimmond and Oke (2002). The surface layer is usually defined to be the lowest 10% of the boundary layer, where turbulent fluxes vary less than 10% in magnitude with height. The surface layer over urban areas can be divided into two sublayers: an inertial sublayer and a roughness sublayer.

The roughness sublayer (RSL) is the region where flow is directly influenced by the roughness elements. In this layer, the turbulence field is inhomogeneous and the flow is

highly irregular. The depth of the RSL from laboratory and field experiments was reviewed by Roth (2000). Raupach et al. (1991) gave a range of RSL height to be 2~5 times the average roughness element height.

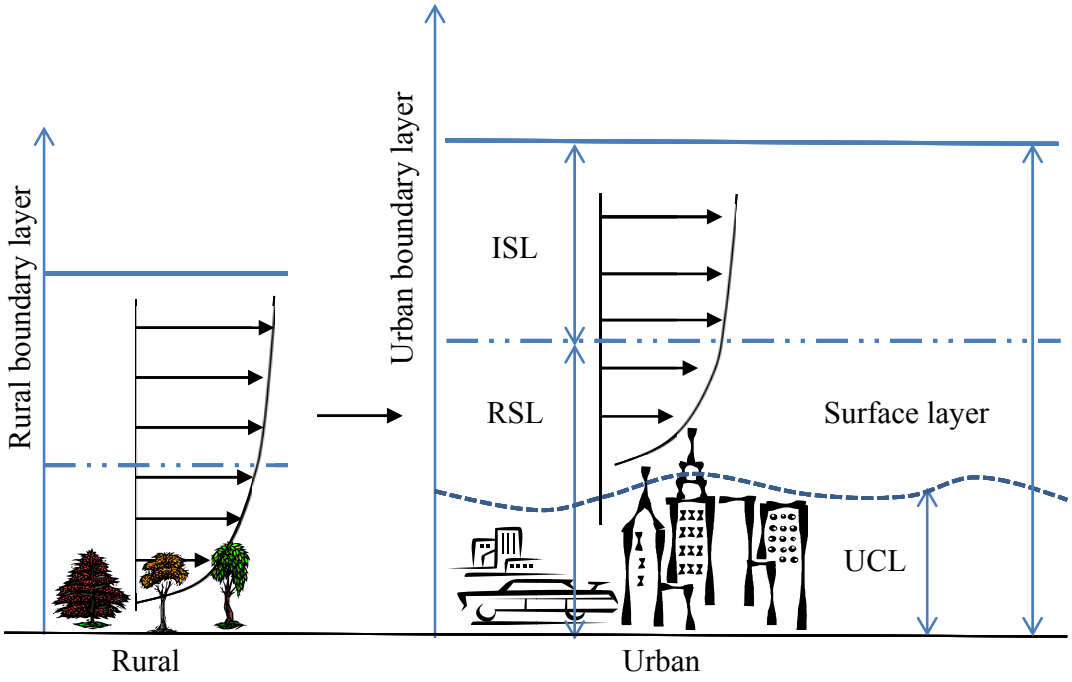


**Figure 1-1. Structures of urban and rural boundary layers (adapted from Grimmond and Oke (2002)).**

The inertial sublayer (ISL) is the region in which the air flow is not influenced by single roughness elements. The flow can be considered to be horizontally homogeneous and the fluxes nearly constant with height. Monin-Obukhov similarity theory (Monin and Obukhov, 1954; Foken, 2006) usually applies to this layer. However, the RSL can be tens of meters over the urban area, while the ISL is "squeezed" or does not exist (Cheng and Castro, 2002).

The urban canopy layer (UCL) is the region below the average building height, and is the lowest part of the RSL. Some researchers, such as Rotach (1993a, 1993b), define the lower boundary of the RSL as the top of the UCL. The micro-scale processes within the street canyons between the buildings dominate the UCL (Oke, 2003). The mean flow and turbulence are controlled by the geometry of immediate buildings and street canyons. Modeling dispersion in the UCL is the primary challenge in estimating the air quality impact of a DG located in an urban area.

### 1.2.2 Field Studies on Urban Dispersion

Several tracer studies have been conducted in urban areas to understand dispersion from a variety of sources. The St. Louis study (McElroy and Pooler, 1968), conducted over the period 1963-1965, consisted of a series of 26 daytime and 16 evening experiments in which fluorescent zinc cadmium sulfide particles were released near ground level at two different locations. The plume dispersion data from St. Louis together with data from other urban tracer experiments conducted in Johnstown, Pennsylvania (Smith, 1967) and Ft. Wayne, Indiana (Csanady et al., 1967) were fitted to power curves by Briggs (1973). These curves, referred to as the McElroy-Pooler curves, are used in EPA models such as ISC3 (USEPA, 1995), to estimate dispersion in urban areas. Venkatram (2005) reanalyzed the St. Louis data to show that a simple dispersion model can explain the observed concentration data if the measured values and wind speed and turbulence at release height are used as inputs.

The Copenhagen experiment (Gryning and Lyck, 1984) was conducted during 1978 to 1979 to investigate the dispersion of tracer released from an elevated source, 115 m high, over an urban area during neutral and unstable conditions. As in the case of the St. Louis study, the ground-level concentrations were described well with a simple Gaussian dispersion model using measured turbulence and wind speeds at release height as inputs.

Recently there have been several urban tracer experiments in European and American cities. URBAN 2000 (Allwine et al., 2002; Hanna et al., 2003) was conducted in Salt Lake City in October 2000 to understand dispersion of pollutants in heavily built up areas. Hanna et al. (2003) found that a relatively simple Gaussian dispersion model explained the behavior of the maximum concentrations when the initial plume spread induced by buildings was accounted for.

Venkatram et al. (2004a) conducted a tracer field study in Barrio Logan, California to understand dispersion in an urban area with buildings of heights less than 10 m. This study showed that observed concentrations could be described by a simple dispersion model in which plume spreads were estimated using turbulent intensities in the upper part of the boundary layer. Gryning and Batchvarova (2005) reached the same conclusion in modeling dispersion of tracers released in two experiments: the Copenhagen experiment (Gryning and Lyck, 1984) in which tracer was released at a height of 115 m in an urban area, and the BUBBLE experiment (Rotach et al., 2004) in which a tracer was released at a height of 20 m, which was just above roof level in a built up area of Basel, Switzerland. The primary conclusion from these tracer studies that one hour averaged concentrations

can be predicted adequately with relatively simple models as long as the micrometeorology in the urban area is characterized well.

However, these field studies do not apply directly to emissions from low level buoyant sources such as a DG fired with gas or diesel. For such sources, plume buoyancy can play a major role in determining ground-level concentrations. This motivated the field study, described in this thesis, to examine the applicability of AERMOD to low level buoyant sources located in an urban area.

### 1.2.3 Past Studies on the Impact of DG on Air Quality

Several studies have examined the impact of DG on air quality at urban and regional scales. Iannucci et al. (2000) evaluated the net air emissions effects from the potential use of cost-effective DG in California. First, the study used information on the available DG technologies and their costs to assess the economic market potential for DG, for both utilities and large commercial/industrial customers in years 2002 and 2010. Second, total emissions were calculated for the selected years, given the estimated market penetration levels for each type of DG, and compared with central-generation only scenario. The study concluded that the current California central generation (CG) mix is so clean that virtually no cost-effective distributed generation source could lower net emissions, even when transmission and distribution electric line losses are included. Fuel cells achieved a marginal market penetration, because of their high cost, but showed great promise because fuel cell air emissions are much lower than central station generation.

Allison and Lents (2002) examined the tradeoff between the increase in emissions associated with urban DG emissions and the decrease in emissions by replacing heating plants with waste heat generated from DG plants. They found that realistic DG scenarios were likely to lead to net increases in emissions in urban areas. These two relatively simple analyses focused on aggregated emissions and did not relate these emission changes to air quality. The results and conclusions of these studies were based purely on the assessment of total emissions and did not account for the impact on air quality of the relocation of emissions from rural areas into populated urban areas.

Researchers at the University of California at Irvine (Medrano et al., 2003; Carreras et al., 2004; Samuelsen et al., 2005; Rodriguez et al., 2006) have performed a detailed examination of the impact of DG emissions on ambient concentrations of both primary and secondary pollutants in the South Coast Air Basin (SoCAB) averaged over scales of kilometers. A major part of their effort was the construction of detailed emission inventories for the year 2010. These inventories accounted for growth in energy demand as well as likely DG penetration scenarios. The DG emissions were spatially allocated in the SoCAB using demographic and land-use information. The air quality impacts of DG were examined by running a comprehensive photochemical model using these emission scenarios as inputs. Because DG emissions contribute less than 3% to the total projected $NO_x$ emissions in SoCAB, and less to the VOC emissions, ambient concentrations of ozone, $NO_2$, and PM are changed by relatively small amounts. The maximum concentrations show almost no change, while the largest changes of about 5% occur during nighttime conditions. These results show that DG penetration, amounting to as

much as 20% of energy growth until 2010, has little effect on secondary pollutants such as ozone and $PM_{2.5}$ concentrations. However, this study did not provide results on the impact of primary DG emissions on scales of less than 5 km because the comprehensive air quality model uses a 5 km by 5 km grid resolution. Thus, emissions are instantaneously mixed through a box that is 5 km by 5 km by 10 m. While this approximation might be valid for estimating secondary pollutants, it cannot provide realistic concentration estimates of primary pollutants at neighborhood scales of meters to kilometers.

Heath et al. (2003; 2006) and Heath and Nazaroff (2007) have examined the air quality impact of DGs relative to CG stations. They found that the air quality impact of DGs, quantified in terms of intake factors, could be several times that of CG stations because a) the ground-level concentrations normalized by emissions from the high stack of a CG plant are much smaller than the corresponding concentrations associated with the near ground emissions from DGs, such as microturbines, and b) CG plants are likely to be located far from populated urban centers, while DGs are located in urban areas close to energy consumers. These conclusions are based on a simple Gaussian model that assumes an effective emission height of 5 m for DGs. As we will see later, this assumption might exaggerate the relative impact of DGs relative to central generating stations with large effective stack heights. Furthermore, the intake fraction used to estimate the relative impacts of the DG and CG stations normalizes the concentrations by the emission rates, which means that comparison of the relative impacts is effectively a comparison of the dispersive abilities of tall CG stacks with much shorter DG stacks. A more realistic

comparison has to account for the fact that CG stations have much higher emission rates than DG stations. Thus, the results from these studies do not directly address the impact of DG emissions relative to emissions from CG stations.

### 1.3 Motivation and Objectives

AERMOD is currently the most widely used dispersion model in the United States because the USEPA recommends it as the model of choice for regulatory applications. AERMOD is also used for non-regulatory applications, such as risk assessment, because it incorporates the state-of-the-art in dispersion and micrometeorology, it is available at no cost and is relatively easy to use. AERMOD has been evaluated extensively with data collected in the vicinity of isolated power plants located in both flat and complex terrain. Although it has been evaluated with ground-level concentrations measured around a power plant located in Indianapolis, its applicability to sources within the UCL has not been tested (See Perry et al., 2005). Past Studies, such as in Barrio Logan (Venkatram et. al., 2004a) and around buildings located in a parking lot (Venkatram et. al., 2004b), indicate that AERMOD type models apply even to complicated situations if meteorological parameters close to the source are characterized well. However, these studies were conducted with inert tracers, which do not mimic the buoyant emissions from a typical distributed generator. Therefore, there is a need to evaluate AERMOD using data collected around a DG and modify the model, if necessary, to allow its application to buoyant emissions from low level sources in urban areas.

The review indicates that there is a need to make direct comparison between the relative impacts of DG and CG on local and regional air quality explicitly accounting for their differences in stack characteristics and emission rates. The comparison must also account for the difference in building geometry, urban and rural meteorology and generator type distributions. Methods are needed to conduct the comparison of air quality impacts of single generators and generator deployments in the short and long terms.

A more realistic assessment of the air quality impact of urban sources, such as DGs, requires a model that can estimate background concentration over multiple scales. In principle, an Eulerian grid model could satisfy this requirement if the grid size is small enough, but such a model would be impractical from a computational viewpoint. Furthermore, at scales of meters, dispersion parameterizations in grid based models are inadequate for resolving the horizontal and vertical structure of plumes. Combination of transport models with chemistry models is needed to estimate background concentrations efficiently over multiple length scales.

The overall objective of the research described in this thesis is to develop methods to estimate the air quality impact of urban sources on multiple scales. The specific objectives are:

a) Evaluate and improve current dispersion models, such as AERMOD, to allow their application to low level buoyant sources, such as DGs, located in urban areas;
b) Use AERMOD, modified if necessary, to evaluate the relative impacts of distributed and centralized generation of electricity on local air quality.

c) Develop and evaluate methods to combine transport models and chemistry models to estimate background concentrations that govern the relative air quality impact of local sources.

## 2. Dispersion of Buoyant Emissions from a Low Level Source in an Urban Area

### 2.1 Introduction

This chapter studies the dispersion of buoyant emissions from a DG in Palm Springs, CA. It is motivated by the need for methods to estimate the air quality impact of a DG at source-receptor distances of tens of meters to kilometers and the need to examine AERMOD's applicability to low level buoyant sources in urban areas. Past studies on dispersion focused on either elevated releases (Venkatram, 1980; Venkatram et al., 1984; Venkatram and Paine, 1985) or surface releases (Venkatram, 1982; Eckman 1994; Venkatram, 2004). The application of these methods to low level buoyant sources has to be examined.

Tracer studies (Smith, 1967; Csanady et al., 1967; McElroy and Pooler, 1968; Gryning and Lyck, 1984; Allewine et al., 2002; Hanna et al., 2003; Venkatram et al., 2004a; Rotach et al., 2004) provide important information on passive releases in an urban area, but they do not apply directly to the emissions from low level buoyant sources such as a DG fired with gas or diesel. For such sources, plume buoyancy can play a major role in determining ground-level concentrations.

Because there is little field data for this type of source, Venkatram et al. (2004b) first conducted a tracer study in a parking lot in which a tracer, $SF_6$, was released from the top of trailer, surrounded by small buildings. The results of the tracer experiment indicated that existing dispersion models, such as AERMOD, do need improvement and can overestimate maximum concentrations and underestimate area-wide concentrations in

urban areas. Recent reinvestigation of Prairie Grass filed study (Barad, 1958a; Barad, 1958b) and Idaho Falls field study (Sagendorf and Dickson, 1974) by Qian and Venkatram (2011) indicates that AERMOD also needs modification under low wind speed conditions, which could be the case when urban buildings are present.

Although AERMOD has been evaluated with data collected around large power plants (See Perry et al., 2005), only one data set was collected from an urban source and the emission was from a high level elevated source. Therefore, we conducted a field study to collect the data required to model dispersion from low-level buoyant sources. It was conducted in Palm Springs, CA on July 2008 to investigate the dispersion of buoyant emissions released from relatively low level sources in urban areas at source-receptor distances of tens of meters to kilometers.

**2.2 Field Study**

The tracer experiment was conducted from July 15$^{th}$, 2008 to July 21$^{st}$, 2008 at the Sunrise Park in Palm Springs, CA. During the experiment, Sulfur hexafluoride ($SF_6$) was released at the same temperature, around 460 K, as the exhaust air from the top of DG stack which is situated at the top of a 15 m by 15 m by 7 m (W by L by H) building surrounded by two major one-storey buildings (40 m by 70 m by 7 m in the south and 40 m by 50 m by 7 m in the east). The releasing rate was around 3.3 kg/hr, and the exit velocity was 11 m/s. The stack itself is 2.3 m high and 0.3 m in diameter. The DG is driven by a 650 KW gas fired IC engine with heat recovery (Jing et al., 2009).

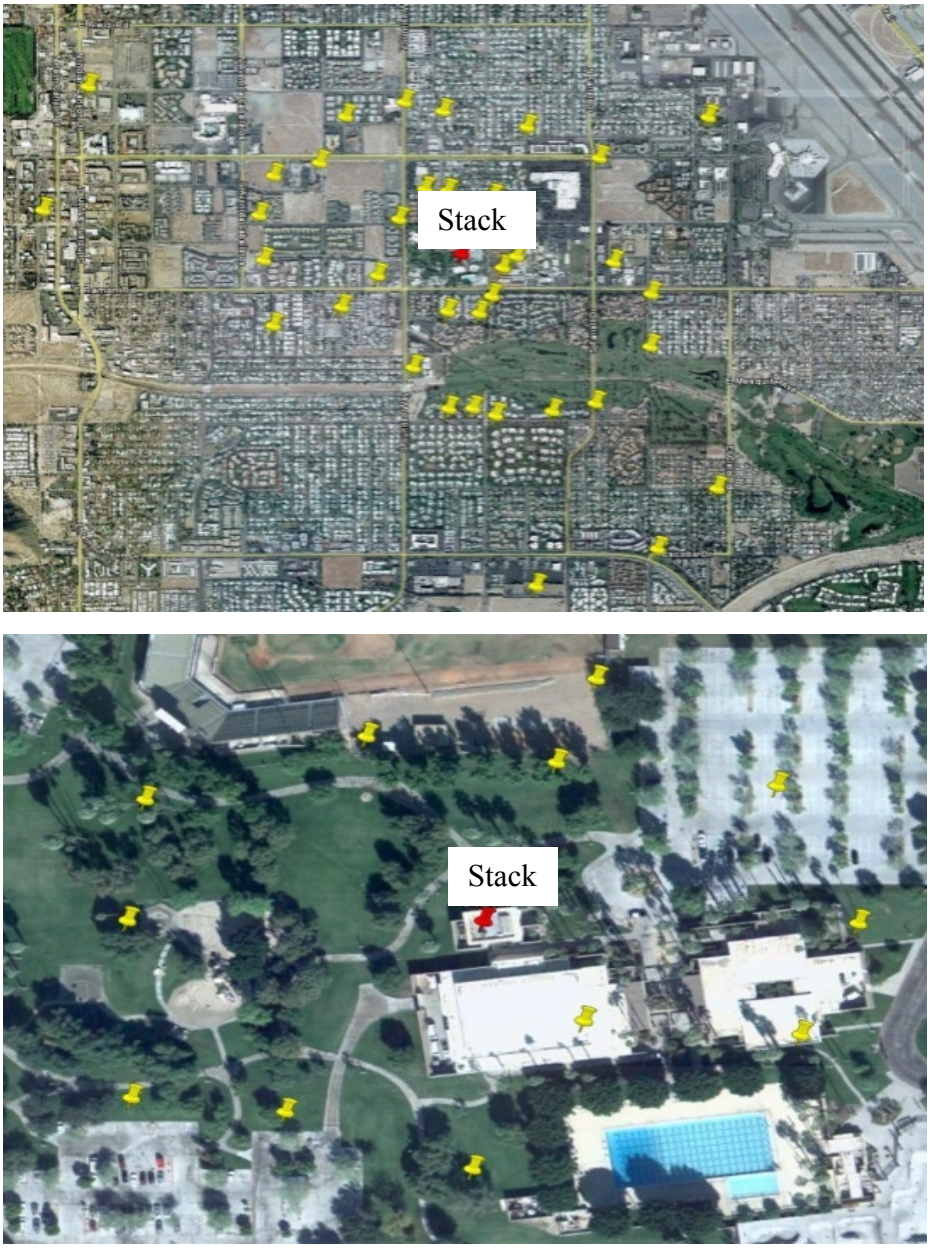


**Figure 2-1. Location of sampling stations and stack. Upper: beyond 100 m from the stack; lower: within 100 m from the stack.**

Figure 2-1 shows locations of the source, the receptors and those three buildings. $SF_6$ concentrations were measured continuously in arcs at distances from 60 m to 2000 m

from the source during the releasing time. At each sampling location, $SF_6$ was draw at a height of 1 m and transferred through polyethylene tubes to a trailer where concentrations were sampled at 5 Hz.

The meteorological station was deployed on a 4-m high tripod located on the roof of the building near the stack. The station consisted of a 3-D Sonic Anemometer and a Krypton Hygrometers at 4 m above the roof, i.e., approximately 11 m above the ground level. The 3-D Sonic Anemometer was pointed toward the true North.

The sonic anemometer sampled the three components of the velocity and temperature at 10 Hz. The $SF_6$ was released continuously over seven 6-hour periods between 15$^{th}$ and 21$^{st}$ July 2008. To see the different boundary condition impact on the dispersion, we made three daytime releases (15$^{th}$, 16$^{th}$, and 17$^{th}$ July 2008, from 09:00 to 15:00 PDT) and four nighttime releases (18$^{th}$, 19$^{th}$, 20$^{th}$, and 21$^{st}$ July 2008, from 01:00 to 07:00 PDT). For analysis, concentrations were averaged over a one-hour period, and meteorological measurements were averaged over a 5-minute period.

### 2.3 Analysis of Observations

#### 2.3.1 Meteorological Observations

Figure 2-2 shows 5-minute averaged meteorological parameters as a function of time of day during the releasing periods. Table 2-1 shows statistics of these meteorological measurements. As shown in the figure and the table, the wind speeds never exceed 3.5 m/s. The 50$^{th}$ and the 95$^{th}$ percentiles indicate that they are below 2.6 m/s during most of the day, and below 1.4 m/s during most of the nighttime. The mean velocities are 1.3 m/s

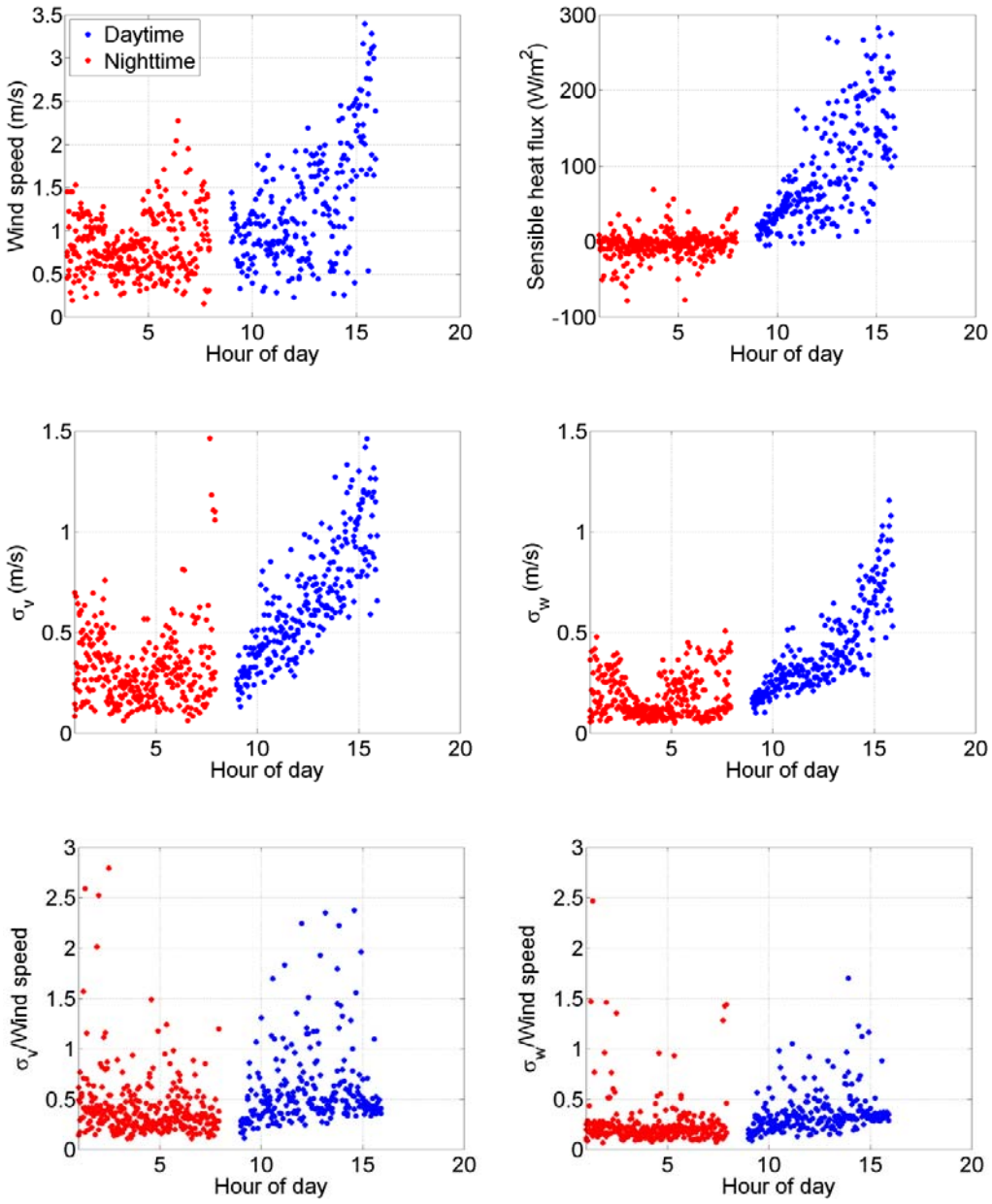


**Figure 2-2. 5-minute averaged meteorological measurements during releasing periods. Upper left: wind speed, (*U*, m/s); upper right: sensible heat flux (*Hs*, w/m$^2$); middle left: lateral turbulent velocity ($\sigma_v$, m/s); middle right: vertical turbulent velocity ($\sigma_w$, m/s); lower left: lateral turbulent intensity ($\sigma_v/U$); lower right: vertical turbulent intensity ($\sigma_w/U$).**

during the day and 0.9 m/s at night. This indicates that the tracer study is a low wind case, especially during the nighttime. Low wind speed conditions are critical because pollutants can build up during these conditions.

Sensible heat flux during daytime goes up to 300 $W/m^2$, which is 88% of the averaged incoming short-wave solar radiation, 342 $W/m^2$. The averaged daytime sensible heat flux is 95 $W/m^2$ upwards, 30% of the averaged incoming short-wave solar radiation. The upward sensible heat flux reinforces the daytime turbulence produced by wind shear. The $50^{th}$ percentiles of lateral and vertical turbulent velocities are 0.3 m/s and 0.6 m/s respectively. The vertical turbulent intensities are above 20% during most of the daytime release periods, and the lateral turbulent intensities are above 30% during most of the daytime.

At night, both upward and downward sensible heat fluxes are observed. The averaged nighttime sensible heat flux is 16 $W/m^2$ towards the ground, which indicates that most of the nighttime releases are under the stable conditions.

Table 2-1 shows that turbulent velocities during the nighttime are less than those during the daytime; however, the turbulent intensities are similar. The relatively low wind speeds and the relatively high turbulent intensities suggest accounting for horizontal meandering in modeling the concentrations during the nighttime.

**Table 2-1. Statistics of 5-minute averaged meteorological measurements.**

| | $U$ (m/s) | | | $Hs$ (W/m$^2$) | $\sigma_w$ (m/s) | | | $\sigma_v$ (m/s) | | | $\sigma_w/U$ | | | $\sigma_v/U$ | | |
|---|---|---|---|---|---|---|---|---|---|---|---|---|---|---|---|---|
| | The percentile | | Mean | Mean | The percentile | | Mean | The percentile | | Mean | The percentile | | Mean | The percentile | | Mean |
| | 50$^{th}$ # | 95$^{th}$ | | | 5$^{th}$ | 50$^{th}$ | | 5$^{th}$ | 50$^{th}$ | | 5$^{th}$ | 50$^{th}$ | | 5$^{th}$ | 50$^{th}$ | |
| Daytime | 1.1 | 2.6 | 1.3 | 95 | 0.2 | 0.3 | 0.4 | 0.3 | 0.6 | 0.7 | 0.2 | 0.3 | 0.4 | 0.3 | 0.4 | 0.6 |
| Nighttime | 0.8 | 1.4 | 0.8 | -16 | 0.06 | 0.1 | 0.2 | 0.1 | 0.3 | 0.3 | 0.1 | 0.2 | 0.3 | 0.2 | 0.3 | 0.5 |

# The 50$^{th}$ percentile is the median.

### 2.3.2 Observed $SF_6$ Concentrations

#### 2.3.2.1 Spatial Variation of Observed Concentrations

During low wind speed conditions, meandering due to mesoscale motions, such as low level jets, mesoscale wind systems, breaking gravity waves and density currents (Salmond and McKendry, 2005), can dominate dispersion in the horizontal. Meandering of the wind cannot be readily related to local measurements, and turbulent velocity fluctuations in the vertical become uncorrelated with the surface friction velocity.

The meandering is reflected in the patterns of $SF_6$ concentrations observed during the experiments. The top panel of Figure 2-3 is typical of the concentrations observed during the daytime. The negative distances refer to upwind receptors. The concentrations drop off with distance as expected, but there are small upwind concentrations up to distances of 1000 m.

The pattern is very different during the night when the wind speeds are low and the turbulent intensities are high. The concentrations are generally higher than the daytime concentrations and do not fall off as rapidly as during the day, and the upwind concentrations are comparable to the downwind concentrations. This suggests that the DG plume is trapped in a relatively shallow boundary layer at night, and is spread in all directions by the meandering wind.

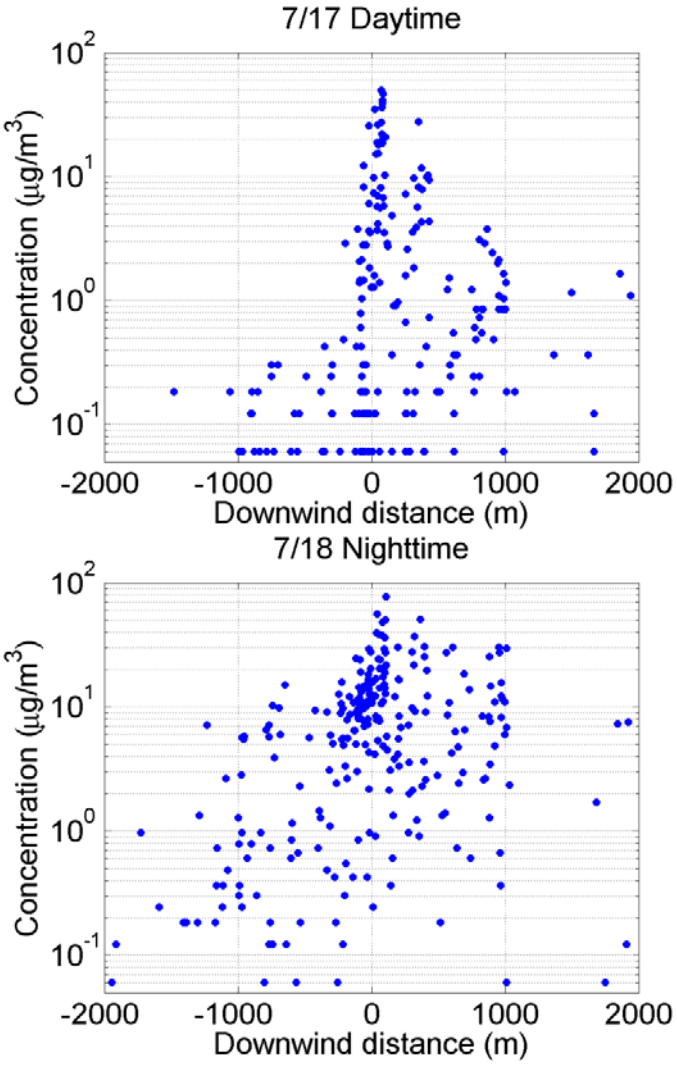


**Figure 2-3. Observed concentrations as a function of downwind distance on 17th, and 18th July, 2008.**

Table 2-2 shows the statistics of observed upwind and downwind concentrations. The maximum concentrations during the daytime and nighttime are comparable, but the median concentrations, both upwind and downwind, are significantly larger during the night. The median of the upwind concentrations, 5 $\mu g/m^3$ is two orders of magnitude larger than that during the daytime. The downwind median concentration during the night

is about ten times larger than that during the day. The maximum concentrations do not differ significantly between night and day at upwind and downwind receptors; the downwind maxima are about two to three times the maxima at the upwind receptors.

**Table 2-2. Statistics of observed daytime and nighttime concentrations**

| | Upwind concentration (µg/m$^3$) | | | | Downwind concentration (µg/m$^3$) | | | |
|---|---|---|---|---|---|---|---|---|
| | percentile | | | Maximum | percentile | | | Maximum |
| | 30$^{th}$ | Median | 95$^{th}$ | | 30$^{th}$ | Median | 95$^{th}$ | |
| Nighttime | 1 | 5 | 18 | 29 | 4 | 8 | 39 | 77 |
| Daytime | 0 | 0.06 | 3 | 26 | 0.2 | 1 | 36 | 50 |

Figure 2-4 shows averaged concentrations as a function of the deviation of the wind directions from the line joining the center of the source to the receptor. These averaged concentrations were obtained by averaging the 6 hours of the measured hourly concentrations over 10º sectors. During the daytime, the highest concentrations occur directly downwind of the emission source, but at angles over 100º, levels less than 10% of the maximum value are observed; at night, the meandering wind spreads the DG plume in all directions, and levels close to 25% of the nighttime maximum value are observed at angles over 100º.

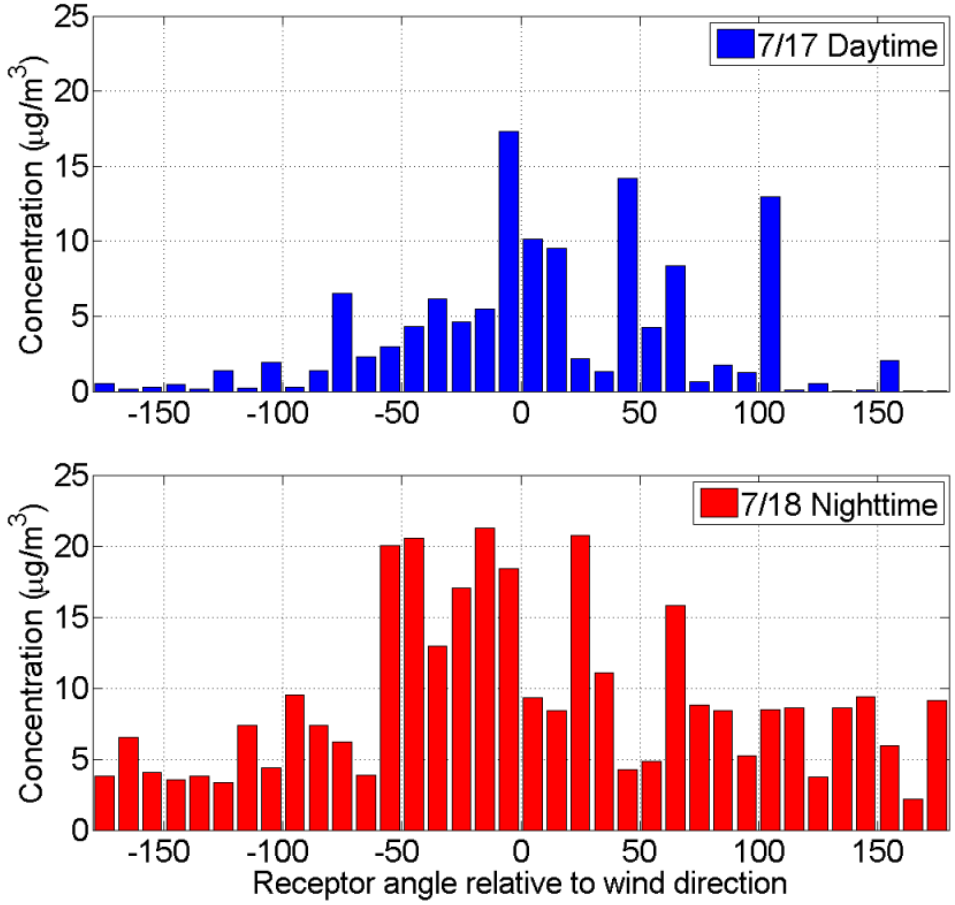


**Figure 2-4. Concentrations as a function of the deviation of the wind direction from the line joining the center of the source to the receptor. Hourly concentrations averaged over 10º sectors.**

Figure 2-5 shows the spatial variation of maximum observed concentrations during all release periods. The daytime observations fall off at a rate which is inversely proportional to the radial distance from the source to the power of 1.4. However, the concentrations fall off slower than the daytime, at a rate of about distance raised to 0.63. Figure 2-5 also shows that some of the observations at 2000 m are close to 10 µg/m$^3$ during the night.

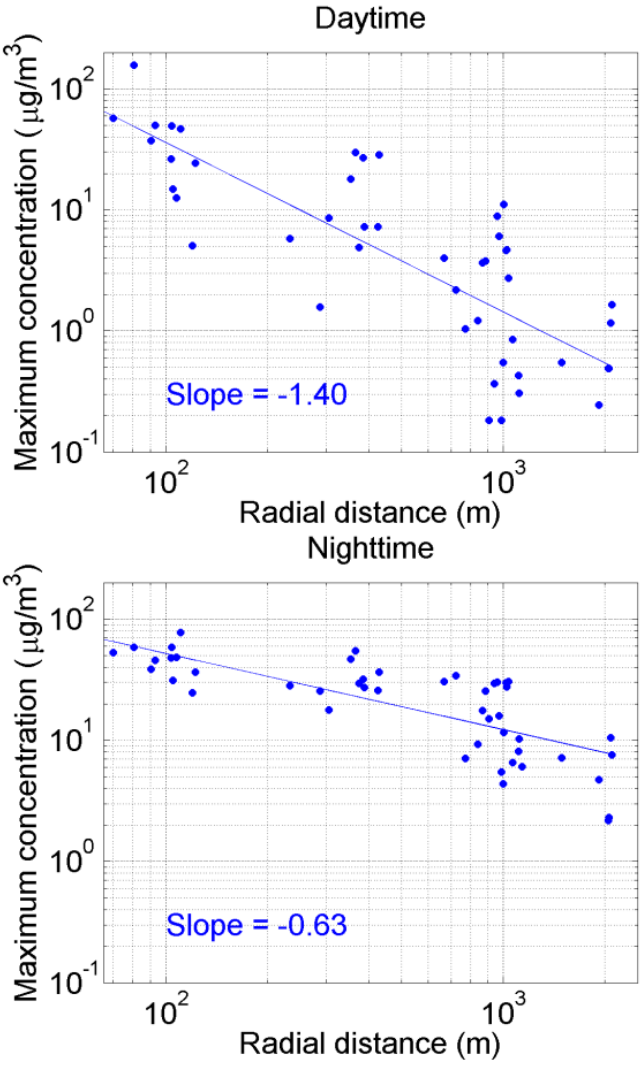


**Figure 2-5. Hourly maximum arc concentrations as a function of radial distance**

### 2.3.2.2 Temporal Variation of Observed Concentrations

It has already been shown in the above analyses that the daytime dispersion pattern is quite different from the nighttime. This section will discuss the concentration differences among daytime or nighttime periods.

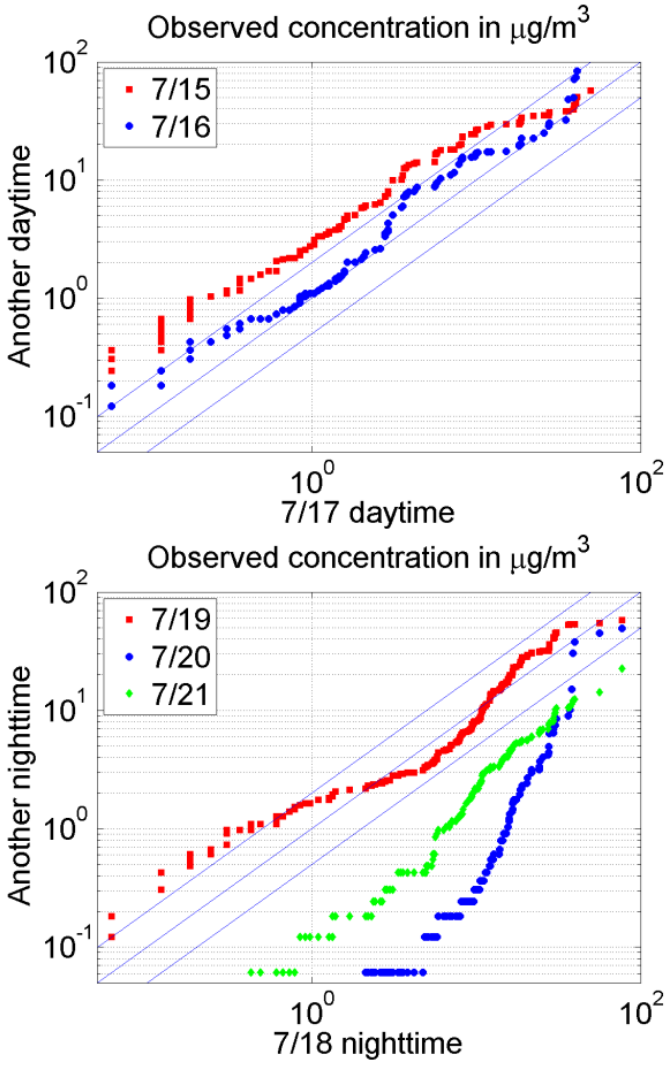


**Figure 2-6. Comparison of observed concentrations among different daytime or nighttime releasing periods using Quantile-Quantile plots.**

Figure 2-6 shows one daytime or nighttime observed concentration against another using quantile-quantile (Q-Q) plots (Venkatram, 1999; USEPA, 2003). The Q-Q figures plot ranked model predictions against ranked observations. The main point of comparing distributions is to minimize the scatter associated with inherent uncertainty. The upper panel shows that there are temporal variations in the daytime concentrations during

different release periods. However, the concentrations vary much more from one night to another. July 20th and July 21st have lower nighttime concentrations than the other two nights, and July 20th has the lowest ones.

Table 2-3 shows that the concentration distribution patterns of July 20th and July 21st are different from the other two nights, and they are similar to daytime patterns. The concentrations during July 20th are smaller than those observed during daytime. However, Table 2-3 does not show distinct differences in stack parameters, emission rates and meteorological measurements. The high concentrations that occur on July 18th and July 19th nights could be related to the trapping of pollutants by a shallow mixed layer, whose height is difficult to estimate. This trapping is plausible because the buoyant and momentum parameters shown in Table 2-3 indicate an average final plume rise of 30 m according to Briggs's equations (Briggs, 1969) assuming a neutral atmosphere.

**Table 2-3. Statistics of variables and concentrations of each releasing period.**

| | $T_s$ [a] (K) | Q [b] (kg/hr) | $F_M$ [c] ($m^4/s^2$) | $F_B$ [d] ($m^4/s^3$) | U [e] (m/s) | | | $\sigma_v$ (m/s) | | | $\sigma_w$ (m/s) | | | Concentration ($\mu g/m^3$) | | |
|---|---|---|---|---|---|---|---|---|---|---|---|---|---|---|---|---|
| | | | | | The Percentile | | Mean | The Percentile | | Mean | The Percentile | | Mean | The Percentile | | Mean |
| | | | | | $5^{th}$ | $50^{th}$ | | $5^{th}$ | $50^{th}$ | | $5^{th}$ | $50^{th}$ | | $50^{th}$ | $100^{th}$ | |
| 7/15 | 438 | 3.3 | 2.7 | 0.8 | 0.5 | 1.1 | 1.2 | 0.3 | 0.6 | 0.6 | 0.2 | 0.3 | 0.4 | 0.8 | 57 | 6 |
| 7/16 | 437 | 3.3 | | 0.8 | 0.5 | 1.2 | 1.4 | 0.3 | 0.6 | 0.7 | 0.2 | 0.3 | 0.4 | 0.3 | 157 | 5 |
| 7/17 | 436 | 2.9 | | 0.8 | 0.4 | 1.2 | 1.4 | 0.2 | 0.6 | 0.7 | 0.2 | 0.3 | 0.4 | 0.2 | 50 | 3 |
| 7/18 | 456 | 3.3 | | 0.8 | 0.3 | 0.6 | 0.7 | 0.1 | 0.2 | 0.3 | 0.06 | 0.1 | 0.1 | 6 | 77 | 9 |
| 7/19 | 461 | 3.3 | | 0.9 | 0.4 | 0.9 | 0.9 | 0.1 | 0.3 | 0.4 | 0.09 | 0.2 | 0.2 | 4 | 59 | 11 |
| 7/20 | 519 | 3.3 | | 1 | 0.3 | 1.1 | 1.1 | 0.1 | 0.4 | 0.4 | 0.09 | 0.3 | 0.2 | 0.2 | 49 | 2 |
| 7/21 | 465 | 3.2 | | 0.9 | 0.4 | 0.6 | 0.7 | 0.1 | 0.2 | 0.2 | 0.05 | 0.1 | 0.1 | 0.9 | 23 | 3 |

[a] $T_s$ is the exit temperature.

[b] $Q$ is the $SF_6$ releasing rate.

[c] Momentum parameter $F_M = v_s^2 D_s^2/4$, where $v_s$ is the exit velocity, and $D_s$ is the stack diameter.

[d] Buoyancy parameter $F_B = g v_s D_s^2 (T_s - T_a)/4/T_s$, where $g$ is the acceleration due to gravity, and $T_a$ is the ambient temperature.

[e] $U$ is the mean wind speed

## 2.4 AERMOD Modeling

AERMOD (AMS/EPA Regulatory Model, Cimorelli et al., 2005) is representative of the new generation of dispersion models based on current understanding of micrometeorology and dispersion. The USEPA recommends its use for regulatory applications. AERMOD is the dispersion component of modeling system that consists of two major components. AERMET is the meteorological processor that converts routinely available meteorological observations into variables such as friction velocity and mixed layer height required by AERMOD. The modeling system also includes two other components whose use is optional: AERMAP, which uses digital terrain data to generate inputs required by AERMOD to account for the effects of terrain on dispersion, and AERSURFACE, which uses land-use data to generate surface data, such as roughness length and Bowen ratio, required by AERMET.

Past Studies, such as in Barrio Logan (Venkatram et. al., 2004a) and around a building located in an urban parking lot (Venkatram et. al., 2004b), indicate that AERMOD type models apply even to complicated situations if meteorological parameters close to the are characterized well. This suggested that AERMOD could be applied to modeling the concentrations observed during the Palm Springs field study if the meteorological inputs close to the source were used.

### 2.4.1 AERMET Performance

AERMET, AERMOD's meteorological processor, is based on a one-dimensional boundary layer model. AERMET estimates the surface heat flux based on the surface

energy balance, which is a function of latitude, surface albedo, Bowen ratio, surface temperature, fractional cloudiness and so on. The surface heat flux, the roughness length, and the wind speed are used in Monin-Obukhov similarity theory to compute the surface friction velocity and the convective velocity scale. The heat flux is used in combination with upper air temperature soundings to compute the variation of mixed layer height during the day. The surface friction velocity is used to estimate the mechanical mixed layer height during the night. The surface parameters and the mixed layer heights are included in AERMET's surface file (.sfc), which is then used in AERMOD to construct vertical profiles of temperature, wind speed, and turbulence using Monin-Obukhov similarity theory (MOST) (See Cimorelli et al., 2005 for details).

In principle, AERMET cannot be applied to an urban area where surface properties vary sharply. However, Princevac and Venkatram (2007), Venkatram and Princevac (2008), and Qian and Venkatram (2011) show that MOST provides adequate estimates of local meteorological inputs for dispersion models if local measured wind speeds and estimates of roughness length are used. Therefore, in this study, AERMET was used to generate the meteorological inputs using meteorological variables measured next to the tracer release.

The wind speeds and temperature information were initially used from the 11 m sonic measurements made onsite. The surface parameters corresponded to those recommended by the South Coast Air Quality Management District, which derived the parameters by applying AERSURFACE to the Palm Springs urban area. These parameters are: roughness length, $z_0$ = 0.509 m; displacement height, $dh$ = 2.5; Bowen ratio, $Bo$ = 1.5,

which is ratio of sensible heat flux to latent heat flux; and albedo, *al* = 0.22. The cloudiness was taken to be constant at 0.75.

AERMET was also applied using National Weather Service (NWS) data derived from wind speeds and temperatures measured at the Palm Springs airport during the field study conducted in 2008. The upper air data for 2008 was downloaded from the National Oceanic and Atmospheric Administration's Radiosonde Database (http://raob.fsl.noaa.gov/) at Miramar NAS (NKX site), which is close to Palm Springs. The surface parameters were the same as those used for the onsite data, except that actual cloudiness data were used.

The outputs from these two different inputs to AERMET were compared with observed values of surface friction velocity and heat flux. Figure 2-7 shows that both approaches, using NWS and onsite data, lead to substantial overestimation of surface heat fluxes during the daytime, suggesting that the recommended Bowen ratio might be too high for the park environment of the Palm Springs site. This overestimation of heat flux has a relatively small effect on the surface friction velocity estimated using onsite wind speeds: the estimated values are within a factor of two of the observed values, which indicates that the surface friction velocity is insensitive to the surface heat flux. Qian and Venkatram (2011) also shows that the overestimation of heat flux at a central urban site or underestimation at a downwind suburban site has little effect on estimating surface friction velocity. The higher airport wind speeds of the NWS data lead to overestimation of surface friction velocity.

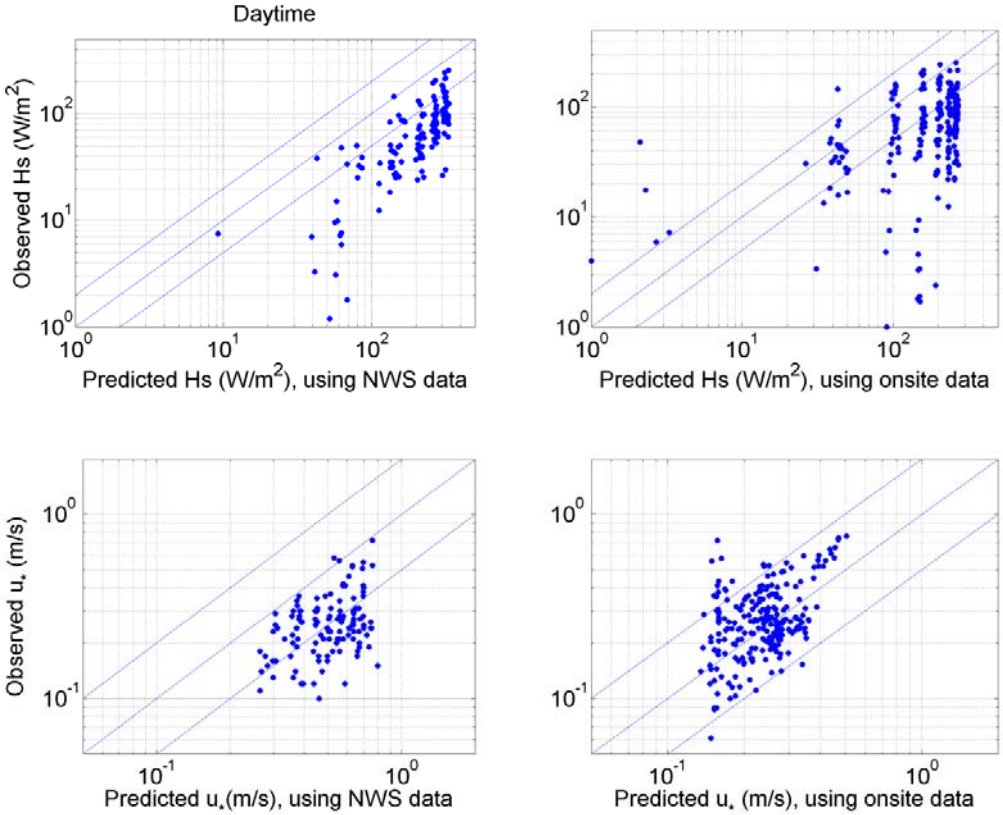


**Figure 2-7. Comparison of AERMET outputs with measurements of heat flux and surface friction velocity made at 11 m during daytime hours.**

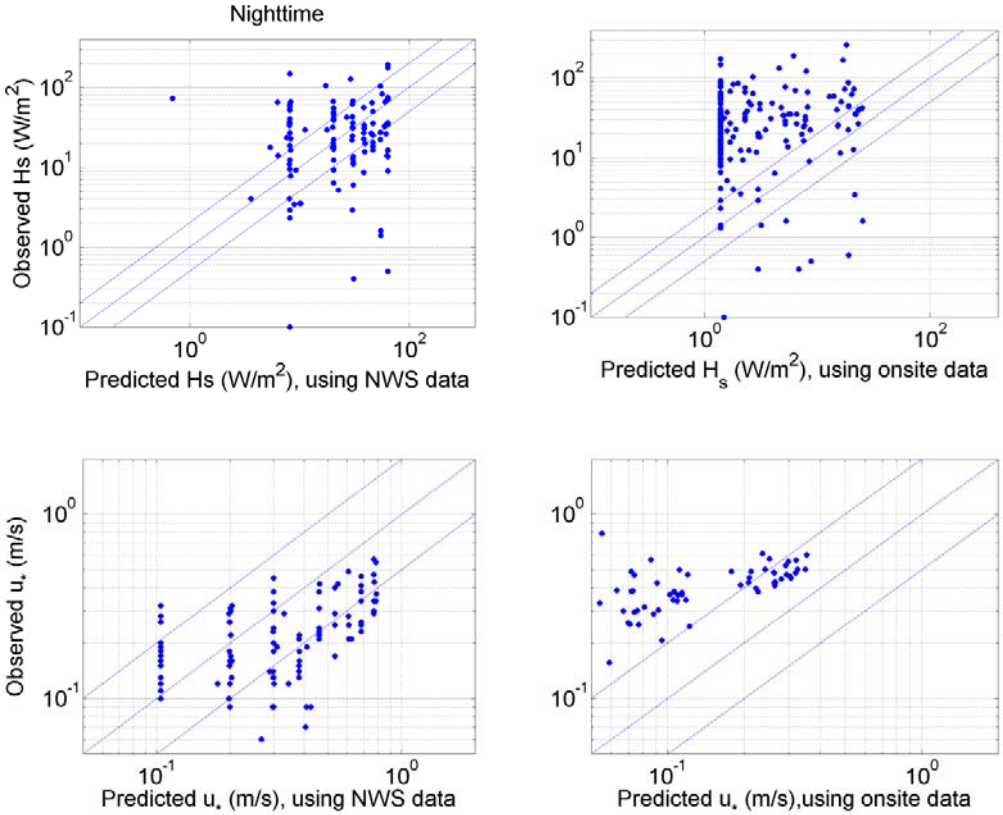


**Figure 2-8. Comparison of AERMET outputs with measurements of heat flux and surface friction velocity made at 11 m during nighttime hours. The absolute values of the heat fluxes, which are primarily negative during the night, are plotted.**

Figure 2-8 shows that using the (incorrect) relatively high wind speeds of the NWS data compensates for underestimation of surface friction velocity by similarity methods due to uncertainty of surface roughness and displacement (Qian and Venkatram, 2010). The NWS data yields more reasonable estimates of surface friction velocity and heat flux (which depends on surface friction) than the onsite data. The surface friction velocity and heat flux are substantially underestimated using the relatively low onsite wind speeds. These results suggest the need for improvements in methods to estimate surface friction and heat fluxes when the wind speeds are relatively low. Because AERMET

underestimates surface friction velocity during nighttime hours, AERMOD was first evaluated with inputs corresponding to measurements from the 11 m sonic anemometer.

### 2.4.2 AERMOD Performance

Although the dispersion formulations in AERMOD are complex (Cimorelli et al., 2005), the core of the model is the Gaussian equation given by:

$$C(x,y,z) = \frac{1}{\sqrt{2\pi}\sigma_z U} H(x,y)\left[exp\left(-\frac{(z-h_{eff})^2}{2\sigma_z^2}\right) + exp\left(-\frac{(z+h_{eff})^2}{2\sigma_z^2}\right)\right], \quad (2\text{-}1)$$

where $\sigma_z$ is vertical spread, $U$ is mean wind speed, $z$ is the receptor height, $h_{eff} = h_s + \Delta h$ is the effective stack height, $h_s$ is the stack height, $\Delta h$ is the plume rise and the $H(x,y)$ is the horizontal distribution. AERMOD modifies the equation to include several effects such as plume reflections from the top of the mixed layer and penetration of the elevated inversion by the buoyant plume.

AERMOD accounts for meandering by defining the horizontal concentration distribution as a linear combination of Gaussian and uniform distributions:

$$H(x,y) = f_p H_p(x,y) + (1 - f_p) H_r(x,y), \quad (2\text{-}2)$$

where $f_p$ is a weighting function, the plume distribution is

$$H_p = \frac{1}{\sqrt{2\pi}\sigma_y} exp\left(-\frac{y^2}{2\sigma_y^2}\right), \quad (2\text{-}3)$$

and the uniform distribution is given by

$$H_r = \frac{1}{2\pi r}. \quad (2\text{-}4)$$

where $r$ is the source–receptor distance. The upwind concentrations predicted by AERMOD result from this meandering algorithm.

We first used onsite meteorological inputs to evaluate AERMOD's performance in predicting concentrations from the low level buoyant source.

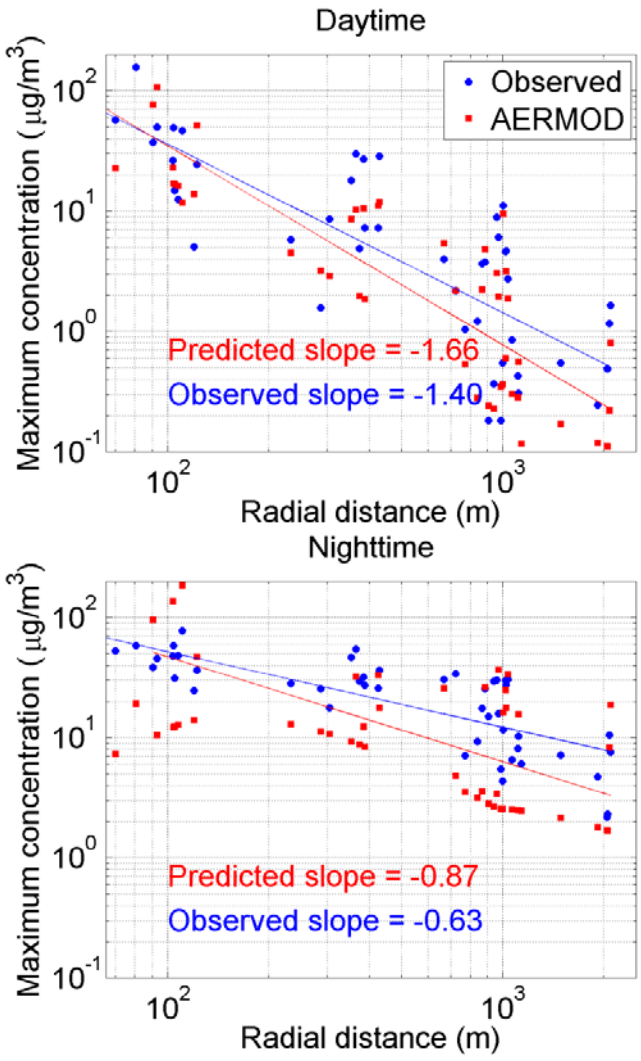


**Figure 2-9. Comparison of predicted and observed hourly maximum arc concentrations as a function of radial distance**.

Figure 2-9 compares the spatial variation of maximum observed concentrations with estimates from AERMOD, when onsite data are used to generate AERMOD inputs. AERMOD predicts a decrease in concentrations with distance that is slightly more rapid

than that observed during the daytime. However, the magnitudes of the estimates are consistent with the observed values during the daytime: the observations and the model estimates fall off by factor of 100 when the receptor distance increases from about 50 to 2000 m, a factor of 40. During the night, however, AERMOD predicts a decrease in concentrations with distance that is much faster than the relatively flat observed decrease. It generally predicts lower concentrations than the observations at distances over 1000 m: some of the observations at 2000 m are close to 10 $\mu g/m^3$ while some of the model estimates are rarely above 2 $\mu g/m^3$. This underestimation could be related to the overestimation of mixing height by AERMET and the overestimation of vertical spread and plume rise.

This tendency to underestimate concentrations during the night at upwind distances over 1000 m is also evident in Figure 2-10, which shows the observed and estimated concentrations as a function of downwind distance from the source for a daytime and nighttime release. Note that AERMOD also predicts upwind concentrations, which is consistent with observed behavior. The upwind concentrations result from the meandering algorithm in AERMOD, which is important in describing the behavior of concentrations in the low wind regimes typical of urban areas.

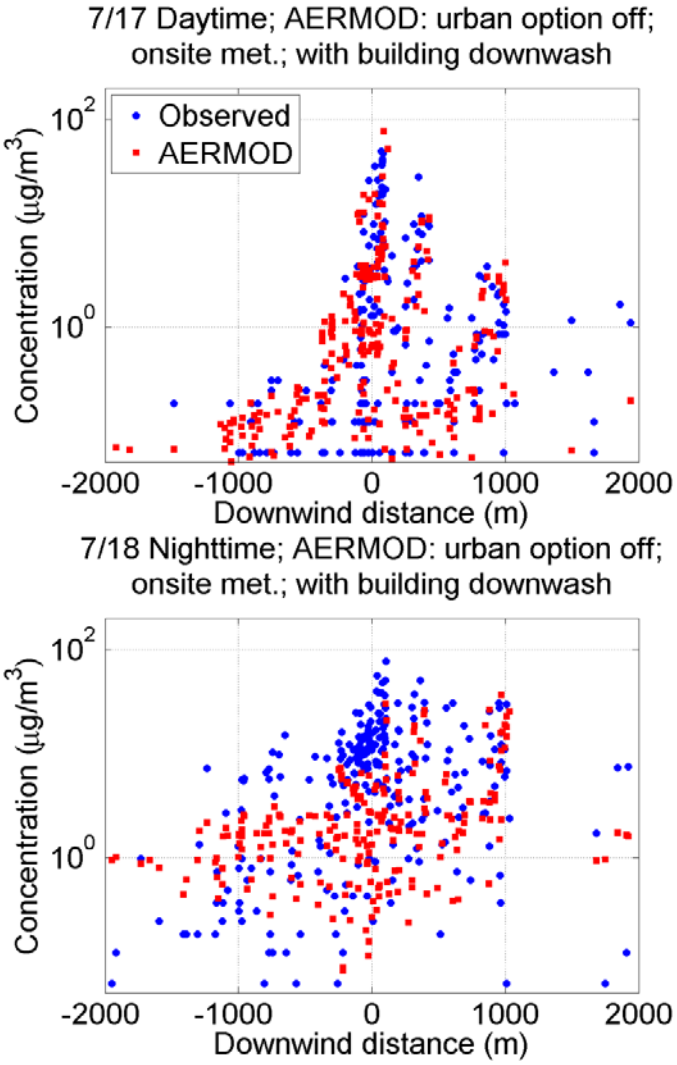


**Figure 2-10. Comparison of predicted and observed hourly averaged concentrations as a function of downwind distance.**

### 2.4.3 Sensitivity Study

This section compares the distributions of observed concentrations with those of estimated values to avoid the inevitable scatter in plots of concentrations paired in space and time. The distributions are compared by the plotting the ranked observations with ranked model estimates.

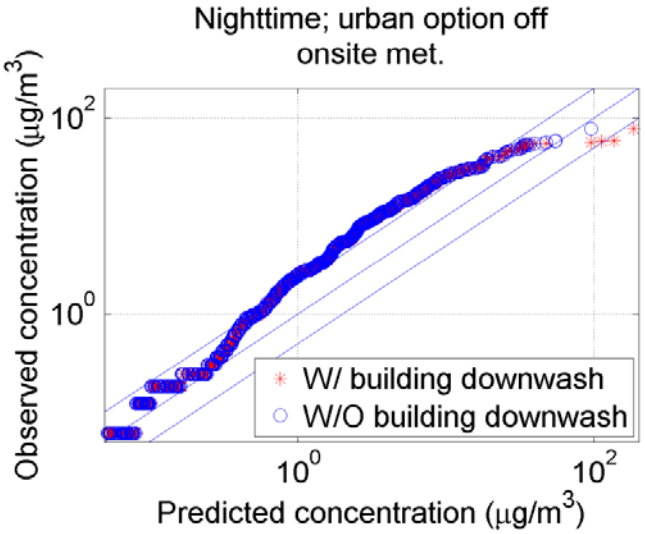


**Figure 2-11. Comparison of observed concentration distribution with that estimated from AERMOD during nighttime conditions when observed heat fluxes, surface friction velocities and horizontal and vertical turbulent fluctuations are used as inputs.**

Figure 2-11 shows the Q-Q plot for nighttime hours when the observed values of surface friction velocity, heat flux, and turbulent levels are used as inputs to AERMOD. AERMOD underestimates the observed concentrations by a factor of two over most of the concentration distribution.

Figure 2-11 shows that the upper end of the concentrations is adequately estimated by AERMOD when building downwash is not included. Including downwash does not affect most of the distribution because the low wind speeds keeps the plume rise high enough, an average final plume rise of 30 m, for downwash effects to be negligible. However, building downwash does affect the few high concentrations that occur near the source and when the plume is still rising. Here the concentrations are overpredicted when downwash is turned on.

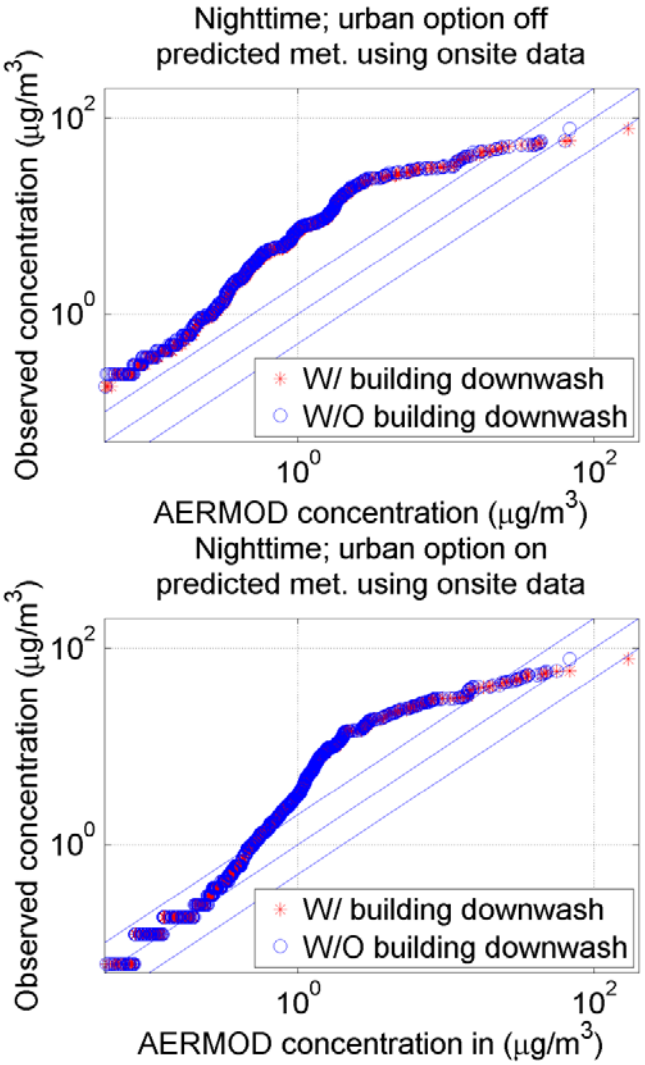


**Figure 2-12. Comparison of observed concentration distribution with that estimated from AERMOD during nighttime conditions when heat fluxes, surface friction velocities, and horizontal and vertical turbulent fluctuations are estimated using onsite data. Upper: urban option off; lower: urban option on.**

This conclusion is supported by the results presented in the upper panel of Figure 2-12, which shows the performance of AERMOD when estimated values of surface friction velocity are inputs. As expected, the underprediction is more severe in most of the distribution, because Figure 2-13 suggests that observed levels of turbulence are higher

than those estimated with similarity theory using observed surface wind speeds as inputs. The high concentrations are overpredicted when downwash is included. The lower panel of Figure 2-12 shows that model performance improves when the turbulence is increased by enhancing the turbulent levels in the urban area.

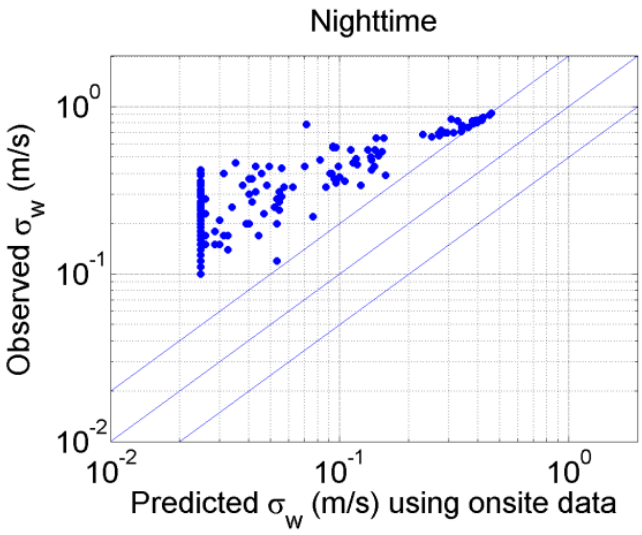


**Figure 2-13. Comparison of observed vertical turbulent velocity ($\sigma_w$) with that estimated from AERMET during stable conditions using heat fluxes and wind speeds measured on site.**

Surprisingly, model performance does not improve when the higher wind speeds of the NWS data are used as inputs, as seen in Figure 2-14. Most of the distribution is underpredicted, while the high concentrations are overestimated. The increase in concentrations associated with higher turbulence levels is compensated by the decrease in concentration caused by higher boundary layer heights. This result suggests that the concentration behavior during the night is a combination of relatively high turbulence levels confined within a shallow boundary layer.

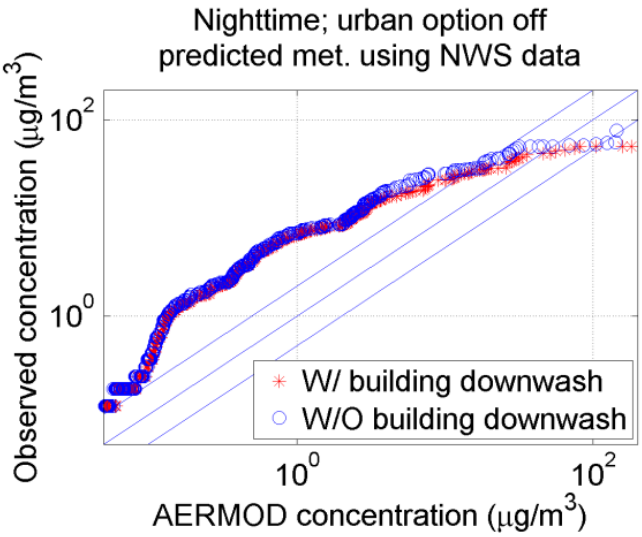


**Figure 2-14. Comparison of observed concentration distribution with that estimated from AERMOD during nighttime conditions when AERMET uses NWS data as inputs.**

Figure 2-15 shows results when mixed layer heights during the night are restricted to 50 m and 120 m. The upper panel shows that there is not much difference between the results for the two mixing heights, and the lower panel indicates that the mixing heights estimated by AERMET are equivalent to fixed mixed layer height of 120 m. The results in the two panels indicate that a shallow mixed layer height, by itself, does not reduce the underprediction in the middle of the distribution.

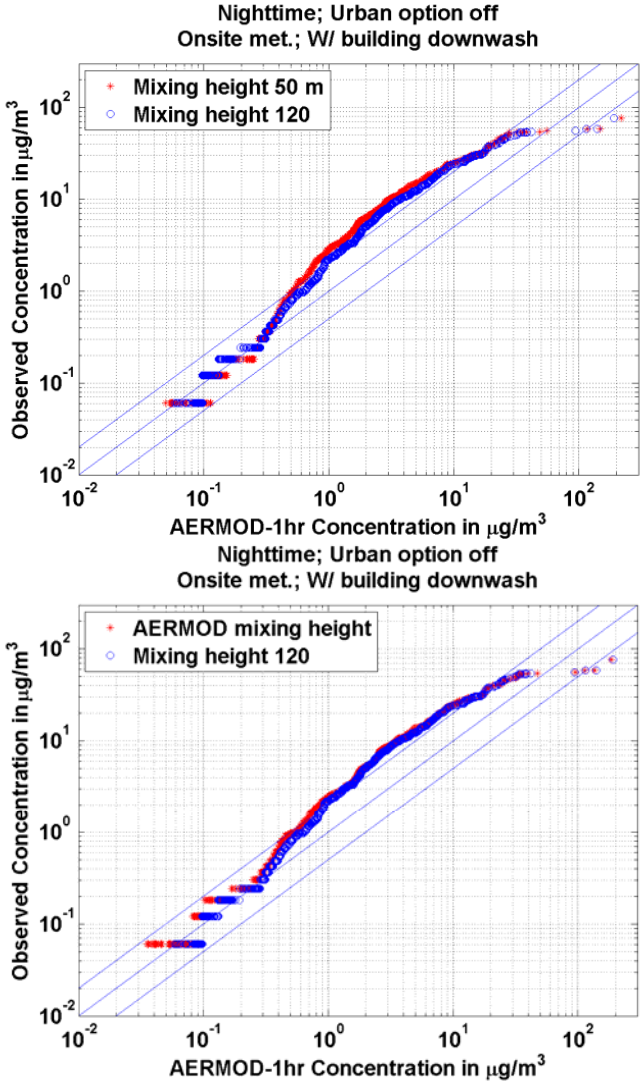


**Figure 2-15. Comparison of observed concentration distribution with that estimated from AERMOD during nighttime conditions when observed heat fluxes, surface friction velocities, horizontal and vertical turbulent fluctuations, and fixed mixing heights are used as inputs.**

### 2.4.4 Modification to AERMOD

The preceding above analysis indicates that using onsite meteorological inputs provide the best description of the nighttime dispersion of low level buoyant sources in an urban

area under low wind conditions. Sensitivity studies show that the nighttime concentration behavior is a combination of relatively high turbulence levels confined within a shallow boundary layer. However, including these still underestimates concentrations. This could be related to the fact that AERMOD assumes symmetric plume growth where the upper part of the plume grows at the same rate as the lower part. This assumption might be unrealistic if the turbulence levels decrease with height so that in combination with the lower wind speeds near the ground, the plume grows much faster towards the ground than towards the top of the mixed layer. These effects can be included by adapting a model proposed by Venkatram and Paine (1985) to describe the dispersion of elevated releases into a shear-dominated boundary layer, which associates two different spreads $\sigma_{zu}$ and $\sigma_{zl}$ with the upper and lower parts of the plume. Their growth of these sigmas is controlled by the turbulence levels at the each of each plume. The growth of the upper and lower plumes is limited by the top of the mixed layer and the ground, so that

$$\sigma_{zu} = min(\sigma_{zu}, z_i - H_e) \tag{2-5}$$

and

$$\sigma_{zl} = min(\sigma_{zl}, H_e), \tag{2-6}$$

where $z_i$ is the mixing height, and $H_e$ is the effective stack height. The vertical spread is then taken to be the average of the upper and lower parts of the plume and is limited by the boundary layer height, thus:

$$\sigma_z = min\left((\sigma_{zu} + \sigma_{ul})/2\,, \sqrt{2/\pi}\, z_i\right). \tag{2-7}$$

Although the stack height of the DG at the Sunrise Park is relatively short, 9.3 m above the ground, plume buoyancy allows the plume to rise 30 m as shown before. Equations

(2-5), (2-6), and (2-7) are used to modify AERMOD. Figure 2-16 shows the results of modified AERMOD. The two plume model results in most of the predicted concentration distribution lying within a factor of two of the observed distribution. However, the upper end of the distribution is overestimated.

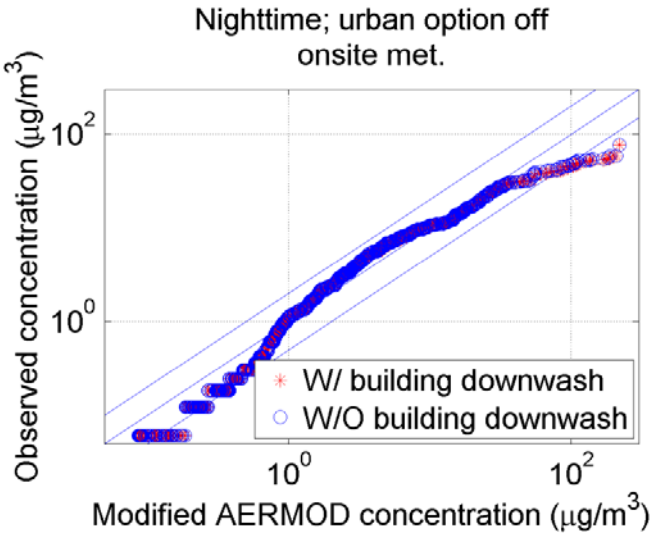


**Figure 2-16. Comparison of observed concentration distribution with that estimated from modified AERMOD during nighttime conditions when observed heat fluxes, surface friction velocities and horizontal and vertical turbulent fluctuations are used as inputs.**

## 2.5 Conclusions

Data from a field study conducted in Palm Springs, CA in the vicinity of a 650 kW power plant were used to evaluate the applicability of AERMOD to modeling concentrations associated with a low level buoyant source located within the urban canopy. Measurements of micrometeorology and concentrations during the nighttime experiments indicate that concentrations observed during the nighttime experiments are generally

higher than those measured during the daytime experiments. They fall off less rapidly with distance than during the daytime.

AERMOD provides an adequate description of concentrations associated with a buoyant release from DG during the daytime when turbulence is controlled by convection induced by solar heating. The inclusion of meandering in AERMOD is important in explaining the occurrence of upwind concentrations during low wind speeds.

AERMOD underestimates concentrations during the night when turbulence is generated by wind shear. In addition, AERMOD predicts a decrease in concentrations with distance that is much more rapid than the relatively flat observed decrease. AERMET, AERMOD's meteorological processor, provides a poor description of the nighttime turbulence levels. Concentration estimates using measured turbulence levels are still a factor of two lower than the observed concentrations. The concentration estimates can be improved significantly by accounting for the different rates of plume growth in the upper and lower parts of the nighttime boundary layer. A modified version of AERMOD that includes this effect using an approach proposed by Venkatram and Paine (1985) provides the best estimates of the nighttime concentrations.

## 3. The Relative Impacts of Distributed and Centralized Generation of Electricity on Local Air Quality in the South Coast Air Basin of California

### 3.1 Introduction

As addressed in chapter 1, past studies either focused on aggregated emissions and did not relate these emission changes to air quality (Allison and Lents, 2002), or did not directly address the impact of DG emissions relative to emissions from CG stations (Heath et al., 2003; Heath et al., 2006; Heath and Nazaroff, 2007). This chapter considers the cumulative impact of distributed generation of electricity relative to that of the centralized generation that it is designed to replace. The region of interest is the South Coast Air Basin (SoCAB) in southern California, covering Ventura, Orange, Los Angeles, San Bernardino and Riverside counties. The geography, meteorology, and the population of the SoCAB have combined together to give rise to poor air quality, which is among the worst in the country, even though automobile emission controls have led to major improvements in air quality over the last thirty years. $NO_x$ emissions from power plants required to accommodate future growth in electricity demand are of concern in view of the recently promulgated one hour federal standard for $NO_2$ of 100 ppb (USEPA, 2010). This is the level that cannot be exceeded by the monitored three year average of the $98^{th}$ percentile of the annual distribution of the daily maxima of the one hour averaged $NO_2$ concentrations. Although current $NO_2$ levels in the SoCAB are below this standard, Los Angeles and San Bernardino counties record levels close to 80 ppb. $NO_2$ monitors placed close to roadways, which is required by the new regulation, might indicate much higher

levels. $NO_x$ emissions from power plants can also increase ozone and fine particulate levels, which still violate state and federal standards in several regions of the SoCAB.

DG using small power plants is one option to reduce the air quality impact of $NO_x$ emissions. In principle, the impact of DG emissions can be minimized by using the waste heat from DG for local heating and cooling and thus offsetting emissions associated with these activities. In this chapter, we do not consider the effects of these emission offsets.

This chapter makes a direct comparison between the relative impacts of DG and CG explicitly accounting for their differences in stack characteristics and emission rates. We estimate the air quality impacts using AERMOD (Cimorelli et al. 2005), which is based on current understanding of dispersion and is recommended by the USEPA for regulatory applications. AERMOD has been evaluated in previous chapter. It provides adequate estimation for maximum ground level concentrations from a low level buoyant source in an urban area. It tends to underestimate concentrations during the night under low wind conditions, but among the 26 meteorological stations for this study, only 5 of them has a median wind speed which is less than 1 m/s (Venkatram et al., 2010). Thus, the focus of this study is the impact of primary emissions at the source-receptor distances of tens of kilometers where a straight-line, steady-state dispersion model, such as AERMOD is applicable.

The primary result of this chapter is a comparison of the relative impacts of CG and DG on air quality in the Southern California Air Basin (SoCAB) of Los Angeles when CG replaces the projected increase of DG by 2010 (Samuelson et al., 2005). Because the

projection was made in 2005 it might not correspond to the actual increase in DG capacity by 2010.

### 3.2 Methods

We use a simple dispersion model to provide preliminary understanding of the relative impacts of CG and DG stations on air quality. We will then refine these calculations using AERMOD (Cimorelli et al., 2005). Assume that a source with an effective stack height of $H_e$ emits at a rate $Q$ into a boundary layer with a height, $z_i$, and constant wind speed, $U$. The maximum ground-level concentration, $C_{max}$, is given approximately by,

$$C_{max} = \alpha\, Q/(h^2 U), \tag{3-1}$$

where $\alpha$ is a constant. So the relative impact of a DG station versus a CG station in terms of the maximum concentration is given by the ratio

$$C_{max}^{DG}/C_{max}^{CG} = (Q^{DG}/Q^{CG}) \cdot (h^{CG}/h^{DG})^2. \tag{3-2}$$

So if emission rates are not taken into account, the impact of a DG is substantially higher than that of a CG because the effective stack height of a DG station is generally much smaller than that of a CG station. Note that the effective stack height of emissions from a DG can be several times the physical height because of the buoyancy of hot exhaust gases.

Once the emitted plumes are mixed through the depth of the atmospheric boundary layer, the effective height of emission becomes unimportant, and the concentration as a function of distance, $r$, from the source is roughly

$$C(r) = Q/(r\theta z_i U), \tag{3-3}$$

where $\theta$ is the angular spread of the plume. We see immediately from this equation that the relative impact is now proportional only to the ratio of the emission rates of the CG and DG stations. This implies that once the plume is mixed by atmospheric turbulence, the DG has a much smaller impact than a CG with a higher emission rate.

The long-term average concentration, $C_{av}(r)$ at a distance $r$ from the source is approximately

$$C_{av}(r) = Q/(2\pi r z_i U). \quad (3\text{-}4)$$

Then, the average concentration that a person is exposed to in moving about in an area that is within a distance $R$ from the source is

$$C_{ex}(R) = \left(\int_0^R C_{av}(r) 2\pi r \, dr\right)/(\pi R^2), \quad (3\text{-}5)$$

which for the simple model works out to be

$$C_{ex}(R) = Q/(z_i U \pi R). \quad (3\text{-}6)$$

Thus, total emission rate plays a major role in determining exposure to pollution of a person moving around within a radius R from the source.

Heath et al. (2006) compare the relative impacts of CG and DG using a metric referred to as the inhalation factor, ***IF***. It is defined as the mass of pollutant per unit time inhaled in air by the population living with a specified radius of the power plant normalized by the emission rate from the plant. In terms of the simple model for dispersion, the expression for IF becomes

$$IF = V_b \int_0^R \rho(r) 2\pi r/(2\pi U z_i)\, dr = \left(V_b \int_0^R \rho(r)\, dr\right)/U z_i, \quad (3\text{-}7)$$

where $V_b$ is the breathing rate, and $R$ is the distance used to define ***IF***. If the population density $\rho(r)$ is taken to be uniform, we can write

$$\rho = P/(\pi R^2), \quad (3\text{-}8)$$

where $P$ is the population within a distance $R$ from the source. With equation (3-7), the inhalation factor becomes

$$IF = (V_b P)/(z_i U \pi R). \quad (3\text{-}9)$$

This simple model suggests that the ***IF*** is primarily a function of the meteorology, and the region R used to define the factor. If we take $z_i$=500 m, $U$= 5 m/s, $V_b$= 12 m$^3$/day, and R=100 km, we obtain,

$$IF \approx 2 \times 10^{-7} P, \quad (3\text{-}10)$$

where $P$ is in millions. The magnitude of ***IF*** is comparable to that presented in Table 1 of Heath et al. (2006), although it does differ in the details. We see that ***IF*** is proportional to the population within 100 km for the source, and is a weak function of source characteristics. Thus, ***IF*** is not an appropriate metric for this study, which focuses on effects of the different source characteristics of DGs and CGs on air quality.

We compare the relative impacts of CG and DG using the measures: 1) the maximum hourly ground-level NOx concentration, which is of regulatory significance, and 2) the annually averaged NOx concentration averaged over a specified scale, which is a crude estimate of exposure to pollution of a person who travels within the specified distance from the source. Comparing an individual CG to a DG is not meaningful because one does not replace the other. The more relevant comparison is one in which the projected increase in distributed power generation is replaced by central generation. This comparison is performed for the South Coast Air Basin.

The representative generating stations used in the simulations are described next.

### 3.3 Generating Stations

#### 3.3.1 Distributed Generators

The physical characteristics of a small DG are modeled after one located at Sunrise Park in Palm Springs, CA. A field study, which was described before, was conducted in the vicinity of this DG to evaluate the performance of AERMOD in describing dispersion of emissions from a small buoyant source located in an urban area. The final plume rise from this source has an average of 30 m under low wind speed, stable conditions, when the ground-level impact is likely to be significant.

The Palm Springs DG is driven by a 650KW gas fired IC engine with heat recovery. The stack of the Palm Springs DG (PS DG) is situated on the top of a 15 m by 15 m by 7 m (W by L by H) building surrounded by two major one-storey buildings (40 m×70 m×7 m and 40 m×50 m×7 m). The stack is 2.3 m high above the roof top, with an inside diameter of 0.3 m. The waste gases exit at a velocity of 11 m/s at a temperature of 460 K.

A 650 kW DG is referred to as 'small', one with a capacity of 2.5 MW is referred to as 'medium', and a 'large' DG has a capacity of 12.5 MW. These sizes are based on the distribution of DGs that are projected to be operated in the SoCAB by 2010 (Samuelsen et al., 2005). Table 3-1 lists the specifics of the DGs examined in our simulations.

In evaluating the impacts of DG on local air quality, we will consider the primary criteria pollutant, $NO_x$, as a surrogate for other pollutants. Unless the emission factors from DGs and CGs are substantially different, this approach provides a reasonable comparison of the relative impacts of CGs and DGs for emissions of primary pollutants.

**Table 3-1. Stack Characteristics and AERMOD results for DGs**

| Generator | Capacity (MW) | $NO_x$ emission factor (g/MWh) | $h_s$[a] (m) | $D_s$[b] (m) | $v_s$[c] (m/s) | $T_s$[d] (K) | Ratio of energy out of stack to capacity | $F_B$[e] ($m^4/s^3$) | $F_M$[f] ($m^4/s^2$) | $C_{av}$[g] (ppt) |
|---|---|---|---|---|---|---|---|---|---|---|
| Palm Springs DG | 0.650 | -- | 9.3 | 0.3 | 11.0 | 460 | 15% | 1 | 3 | -- |
| Small DG | 0.625 | 120 | 9.3 | 1.5 | 3.0/3.3[h] | 450/773[h] | 100%/200% [h] | 6/11[h] | 5/6[h] | 3/2[h] |
| Medium DG | 2.5 | 120 | 10.3 | 1.8 | 8.2/9.1 | 450/773 | 100%/200% | 22/45 | 55/66 | 5/4 |
| Large DG | 12.5 | 101 | 11.3 | 2.6 | 19.6/21.9 | 450/773 | 100%/200% | 111/223 | 653/789 | 10/9 |

[a] $h_s$ = Stack height;
[b] $D_s$ = Stack diameter;
[c] $v_s$ = Exit velocity of exhausted air;
[d] $T_s$ = Exit temperature of exhausted air;
[e] Buoyancy parameter $F_B = g v_s D_s^2 (T_s - T_a)/T_s/4$, where $g$ is the acceleration due to gravity and $T_a$ is the ambient temperature;
[f] Momuoentum parameter $F_M = v_s^2 D_s^2/4$;
[g] Concentrations are associated with a 5 km by 5 km grid square with DGs stand in the center, and meteorological data are from Fontana meteorological station;
[h] With and without the heat recovery.

The exit gas temperatures for DGs are obtained from vendors listed in "California Distributed Energy Resources Guide" (CEC, 2006), which are about 773 K, regardless of plant capacity (Venkatram et al., 2010). With heat recovery (50% efficiency), the exit gas temperatures are taken to be 450 K for all DGs. The building housing the DGs is taken to be 13 m by 25 m by 8 m, with the stack located at the center of the roof top.

The ratio of power out of a stack to the DG's output is taken to be unity for all DGs when heat recovery is considered. This assumes that the efficiency of a DG is 33%, heat recovery efficiency is 50%, and there is no other heat loss. Notice that the Palm Springs DG vents only 15% of its capacity through the stack, which suggests a 78% heat capture efficiency. In the simulations described in this chapter, we use a more realistic heat recovery of 50% for a small generator.

Table 3-1 also lists the momentum parameters and buoyancy parameters. Using these parameters and assuming that the wind speed at stack height is 3 m/s, Briggs's equations (Briggs, 1969) are used to estimate the final effective stack height: In the absence of heat recovery, the large DG has the highest value of 347 m, and the lowest value, 16 m for the Palm Springs DG, is about three times the 5 m assumed by Heath and Nazaroff (2007). In the presence of heat recovery, both exit velocities and exit temperatures decrease, which results in lower final effective stack heights. Note that if the wind speed is lower, the final effective stack heights will be higher:

### 3.3.2 Central Generating Stations

Information on CG stations is taken from the latest USEPA eGrid (USEPA, 2008), and is presented in Table 3-2. The total capacities are provided by California energy commission (CEC, 2009). The capacity factors are taken from the eGrid and the stack parameters and the emission data are taken from the 2002 national emission inventory (NEI) of point sources for criteria air pollutants (USEPA, 2007). We selected CG stations using the following rules: 1) Stations are in the South Coast Air Basin, and are listed in both eGrid and NEI; 2) Total capacity of the CG station is larger than 50 MW; 3) Stations have NOx emissions.

Table 3-1 and Table 3-2 present source information on the CGs and DGs considered in this study. We also provide estimates of annual concentrations averaged over a 5 km grid for each of generators, as a measure of air quality impact. Before we discuss these numbers, we provide a brief description of AERMOD (Cimorelli et al., 2005), the dispersion model that was used to estimate these concentrations.

## 3.4 Modeling Air Quality Impacts

The previous chapter has evaluated AERMOD using tracer data. The limited comparison of observed to modeled concentrations indicates that AERMOD provides adequate estimates of the magnitudes of concentrations caused by buoyant emissions from small power plants located in urban areas. Note that although emissions from the Palm Springs DG have $1/6^{th}$ of the buoyancy of that assumed for a small generator, the plume rise is only half of that for a small generator because plume rise is proportional to the $1/3^{rd}$

**Table 3-2. Stack Characteristics and AERMOD results for CGs.**

| Generator | Total capacity (MW) | Capacity factor | $NO_x$ emission factor (g/MWh) | $h_s$ [a] (m) | $D_s$ [b] (m) | $D_{se}$ [c] (m) | $v_s$ [d] (m/s) | $T_s$ [e] (K) | Ratio of energy out of stack to capacity | $F_B$ [f] ($m^4/s^3$) | $F_M$ [g] ($m^4/s^2$) | $C_{av}$ [h] (ppb) |
|---|---|---|---|---|---|---|---|---|---|---|---|---|
| Alamitos | 1970 | 0.0779 | 236 | 61.1 | 4.4 | 10.8 | 24.7 | 401 | 10% | 1812 | 17780 | 2 |
| El Segundo | 1020 | 0.1109 | 114 | 61.0 | 4.0 | 7.9 | 24.2 | 401 | 11% | 961 | 9239 | 0.5 |
| Harbor | 597 | 0.0734 | 206 | 53.3 | 4.8 | 6.7 | 23.0 | 454 | 17% | 881 | 5986 | 0.6 |
| Haynes | 1724 | 0.2380 | 61 | 73.5 | 7.0 | 17.3 | 13.9 | 386 | 15% | 2314 | 14444 | 0.5 |
| Huntington Beach 1 | 507 | 0.1998 | 46 | 61.9 | 5.2 | 7.4 | 26.2 | 401 | 20% | 904 | 9405 | 0.1 |
| Huntington Beach 2 | 507 | 0.1998 | 69 | 61.9 | 5.2 | 7.4 | 26.2 | 401 | 20% | 904 | 9406 | 0.2 |
| Mountainview | 1054 | 0.0153 | 49 | 39.6 | 3.0 | 7.5 | 9.9 | 392 | 3% | 323 | 1355 | 0.3 |
| Placerita | 120 | 0.0165 | 437 | 25.9 | 3.8 | 6.6 | 23.0 | 412 | 65% | 683 | 5780 | 0.1 |
| Redondo Beach | 1343 | 0.0372 | 583 | 61.0 | 5.1 | 10.4 | 15.2 | 416 | 10% | 1139 | 6216 | 4 |
| Scattergood | 803 | 0.1464 | 32 | 99.0 | 6.9 | 12.0 | 12.7 | 408 | 17% | 1201 | 5765 | 0.1 |

[a] $h_s$ = Stack height;
[b] $D_s$ = Stack diameter;
[c] $D_{se}$ =Equivalent stack diameter;
[d] $vs$ = Exit velocity of exhausted air;
[e] $T_s$ = Exit temperature of exhausted air;
[f] Buoyancy parameter $F_B = g v_s D_{se}^2 (T_s-T_a)/T_s/4$, where $g$ is the acceleration due to gravity and $T_a$ is the ambient temperature;
[g] Momentum parameter $F_M = v_s^2 D_{se}^2/4$;
[h] Concentrations are associated with a 5 km by 5 km grid square with DGs stand in the center, and meteorological data are from Fontana meteorological station.

power of the plume buoyancy under stable conditions when ground-level concentrations are significant.

The average concentrations presented in Table 3-1 and Table 3-2 were estimated with AERMOD using meteorological inputs corresponding to measurements made at the Fontana station maintained by the South Coast Air Quality Management District (SCAQMD). Figure 3-1 shows the locations of the 26 meteorological stations operated by the SCAQMD. Data from these stations have been processed by SCAQMD to generate AERMOD input files, which are archived for use by the public. We used the data corresponding to 2007. We chose Fontana for the calculations presented in Table 3-1 and Table 3-2 because the median wind speed was relatively high, which as shown in the next section results in high concentrations for the buoyant emissions considered here.

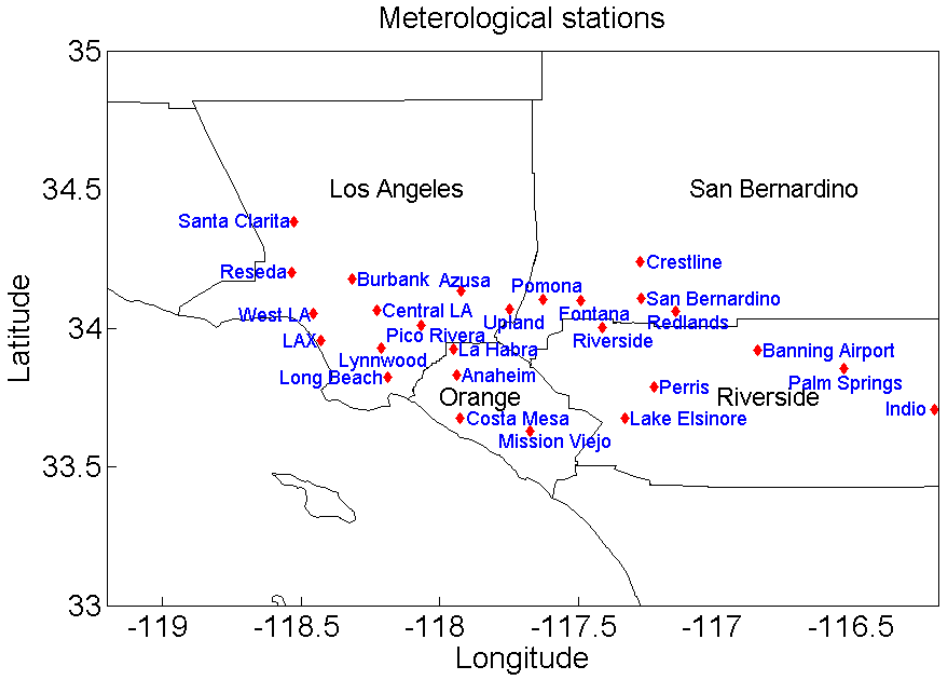


**Figure 3-1. Locations of 26 SCAQMD meteorological stations**

### 3.4.1 Impact of Single Generators

This section examines the air quality impact of a single generator on local air quality. Because wind speed is an important parameter in determining the magnitudes of $C_{max}$ as well as $C_{av}(r)$, we calculated the impacts using two sets of meteorological inputs corresponding to stations with widely differing wind speed distributions. Data corresponding to Pomona and Fontana meteorological stations for 2007 were taken from the SCAQMD archive (SCAQMD, 2009a). These two sets of meteorological data represent low and high wind speed conditions. The maximum, the 95$^{th}$ percentile and the median wind speeds at Pomona meteorological stations are 4.4 m/s, 2.9 m/s and 0.6 m/s respectively, while those at the Fontana meteorological stations are 15 m/s, 6.8 m/s and 1.9 m/s respectively.

A nominal emission factor of $NO_x$ of 32 g/MWh, the California emission standard for new generators, is used in the simulations. The receptors for these simulations are placed on arcs ranging from 1 m to 50 km from the source, and receptors on each arc are 3 degrees apart.

The ground-level concentration increases with emission rate, and decreases with increases in plume rise. An increase in wind speed has two effects: increases dilution and thus decreases ground-level concentrations, decreases plume rise and thus increases ground-level concentration. Thus, estimating the impact of changes in wind speed, heat recovery and power output on maximum ground-level concentrations is not straightforward. Figure 3-2 illustrates the complex relationships, where the ground-level concentrations are estimated using a nominal emission factor of 32 g/MWh.

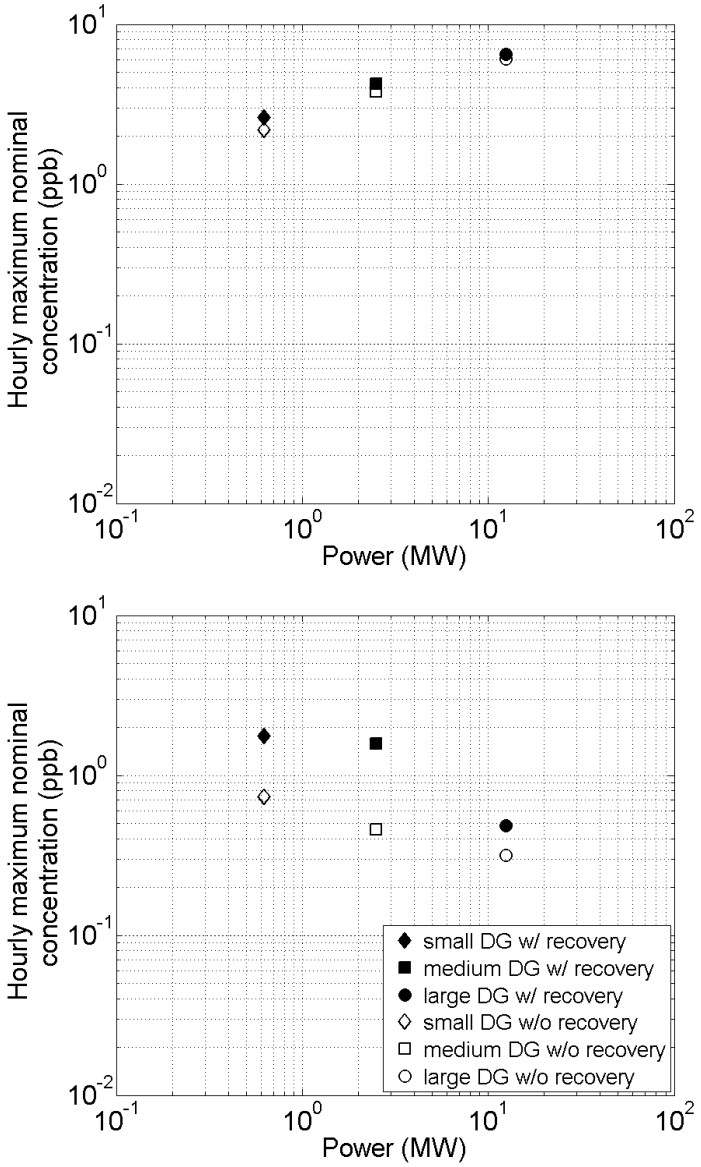


**Figure 3-2. Hourly maximum $NO_x$ concentration of DGs with and without heat recovery. Top panel: Fontana meteorological station-High wind speed; Bottom panel: Pomona meteorological station-Low wind speed.**

The top panel corresponds to the high wind speeds of the Fontana station, while the bottom panel corresponds to the low wind speeds of the urban Pomona station. We see

that the higher wind speeds are associated with concentrations that are higher than those at the lower wind speeds, which indicates the dominance of the effect of wind speed on plume rise.

One expects that as the power increases, the associated increase in emission rate would result in higher maximum concentrations. This is what we see at the high wind speed station, Fontana, where plume rise is kept small. Heat recovery has a small effect on ground-level concentrations because plume rise does not play a role once it is suppressed by the high wind speeds.

When the wind speeds are low, plume rise plays a major role in controlling concentrations. Increased power results in increased plume buoyancy which has a greater impact than increased emissions on ground-level concentrations. Thus, maximum ground-level concentration decreases with increase in power. Furthermore, heat recovery has a major impact on ground-level concentrations for the small and medium DGs: the maximum concentration decreases by about 50%.

Figure 3-3 shows that most CGs produce hourly maximum nominal $NO_x$ concentrations that are at least a factor of two higher than those of DGs because of the much higher emissions from CGs. Unlike DGs, the hourly maximum nominal $NO_x$ concentration from CGs is dominated by the emission rate because the normalized concentration, as seen earlier, is insensitive to stack parameters and is controlled by meteorology. Figure 3-3 shows that the maximum concentration generally increases with power output.

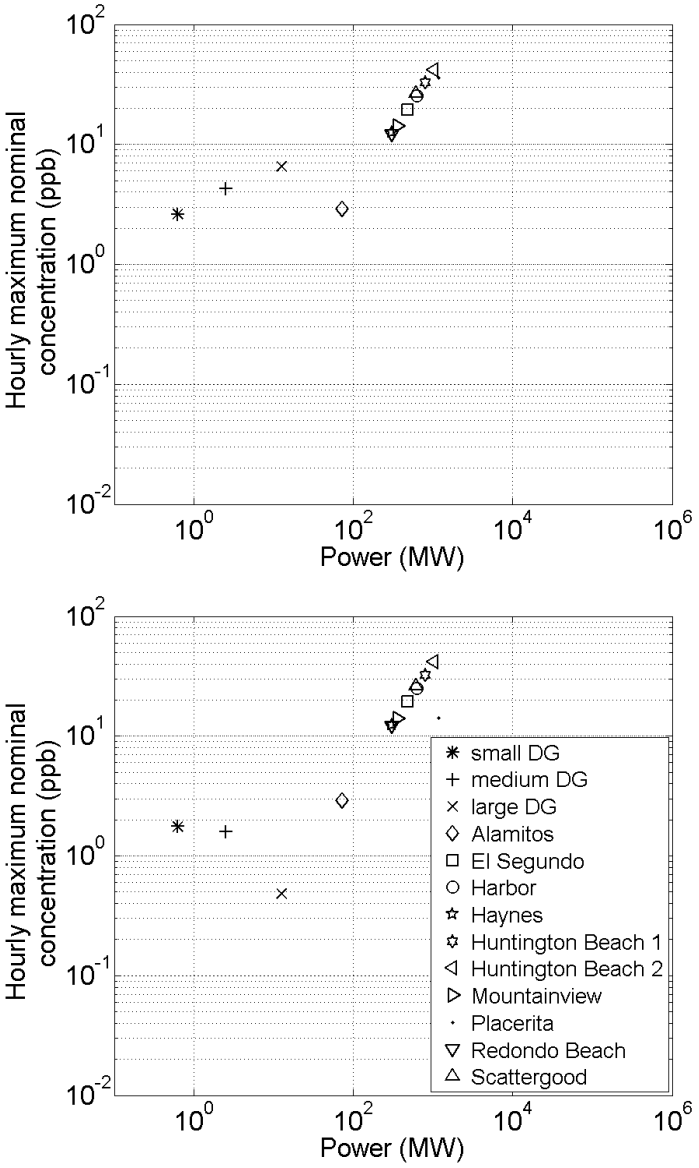


**Figure 3-3. Hourly maximum nominal $NO_x$ concentrations associated with different generators. Top panel: Fontana meteorological station (High wind); Bottom panel: Pomona meteorological station (Low wind).**

Figure 3-4 shows the average concentration of $NO_x$ caused by DGs within a radial distance of 50 km from the source. Note that this average concentration is a crude measure of the exposure to pollution of a person moving within a distance of 50 km from

the source. Because plume rise does not play a role here, the average concentration is determined primarily by dilution and emissions: the average concentration is lower for higher wind speeds and increases with power output. Heat recovery has a minor impact on average concentration.

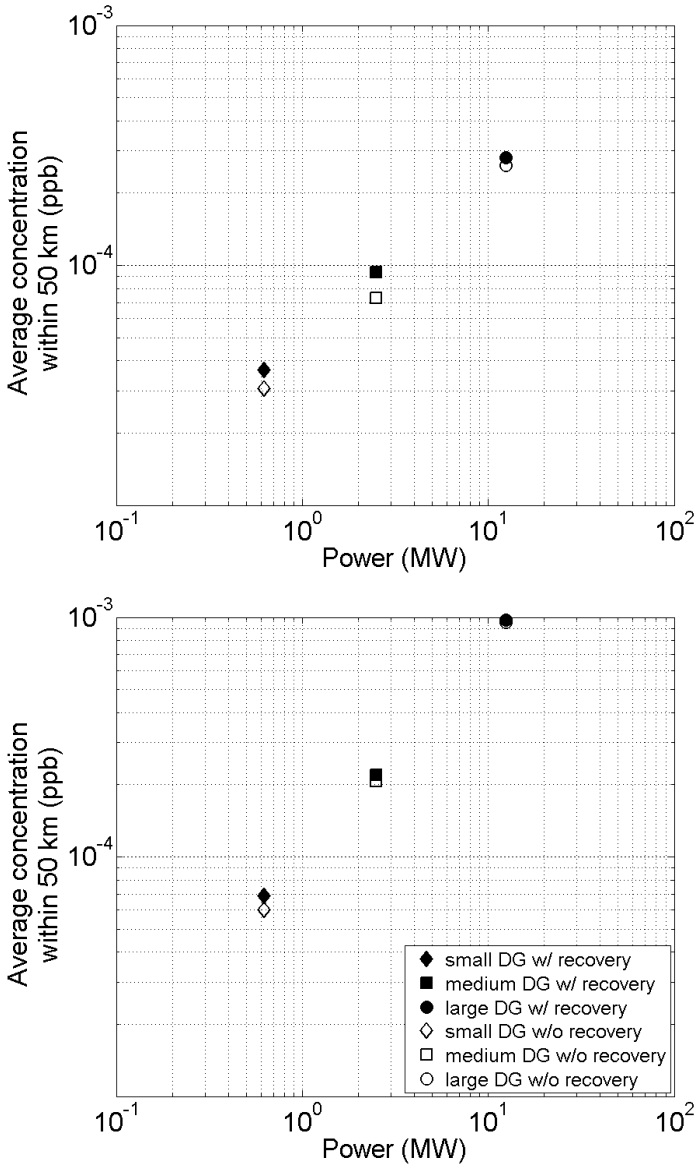


**Figure 3-4. Average concentration of $NO_x$ due to DGs with and without heart recovery. Top panel: Fontana meteorological station; Bottom panel: Pomona meteorological station.**

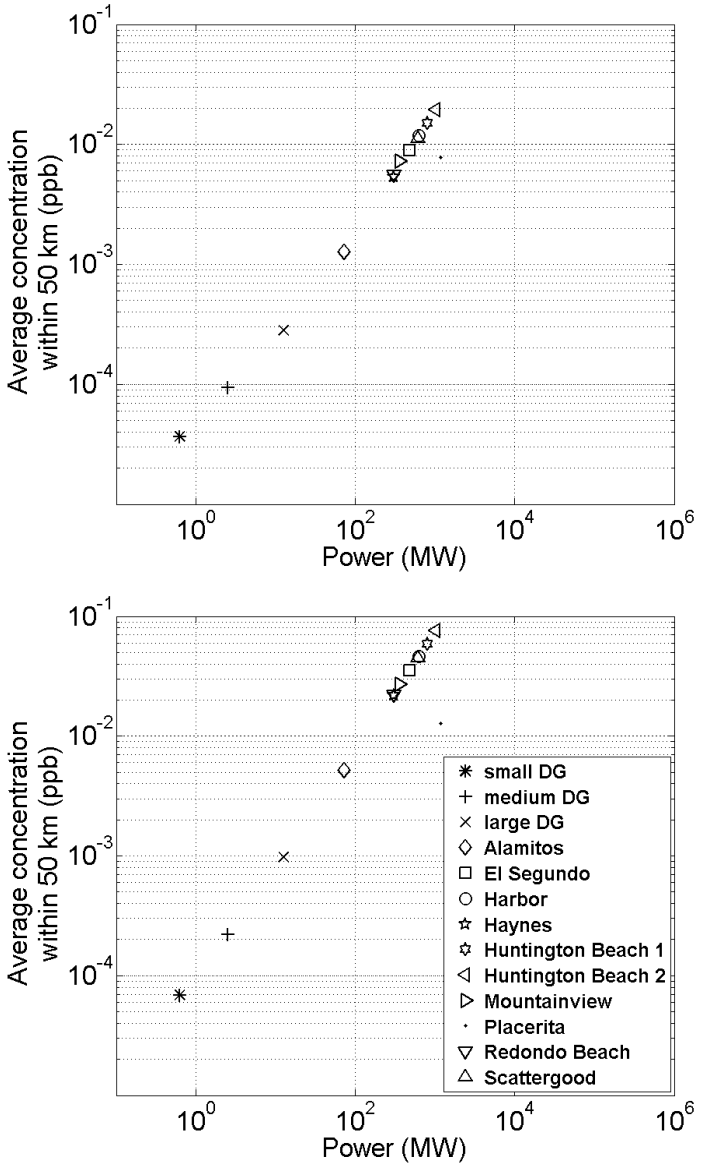


**Figure 3-5. Average concentration of $NO_x$ due to different generators. Top panel: Fontana meteorological station; Bottom panel: Pomona meteorological station.**

Figure 3-5 shows the average concentration of NOx within a radial distance of 50 km from the source as a function of generator type. Like DGs, the average concentration due to CGs is insensitive to the effective stack height, and increases with the increase of the

power and the decrease of the mean wind speed. Figure 3-5 indicates that the average concentration due to most CGs is at least a factor of twenty higher than that due to DGs because of much higher emissions from CGs.

### 3.4.2 Comparing the Relative Impacts of a DG and CG Deployment in the SoCAB

This section compares the air quality impact of penetration of DGs relative to the central generating stations that supply most of the power to Southern California. The comparison is performed by assuming that the responsible agency has the choice between two scenarios: 1) Expand existing CGs to produce the extra power corresponding to the Extra High Penetration (EHP)scenario, 5781 MW, for DG in 2010 (Samuelsen et al., 2005), and 2) Produce the extra power only through DGs. The air quality impacts of these two scenarios are compared by assuming that both DGs and CGs meet the California $NO_x$ emission standard for a new generation device, 32 g/MWh, which translates into a $NO_x$ emission rate of 4.44 tons/day. The increase in power at each CG is assumed to be inversely proportional to its current capacity. This assumes that the smaller CGs have more room to expand. Other assumptions about the power distribution make little qualitative difference to the results, described next.

Figure 3-6 shows the locations of the current CGs in SoCAB listed in Table 3-2. Among these 10 facilities, only the Placerita facility is located in a rural area, while all the other CGs are located in urban areas. These CGs have a total power output of 9644 MW, and emit $NO_x$ at a rate of 42.75 tons/day assuming that they operate all the time.

The EHP (Samuelsen et al., 2005) scenario for DGs corresponds to a power of 5781 MW: 39% is produced using advanced gas turbines (small and medium DGs in Table 1, 52% is produced using conventional gas turbine (large DGs in Table 1), and 9% through fuel cells. The total $NO_x$ emission rate from this combination of DGs is 13.76 tons/day. The large DGs are located in industrial areas, while the densities of the medium and small DGs correlate with population densities in the LA basin.

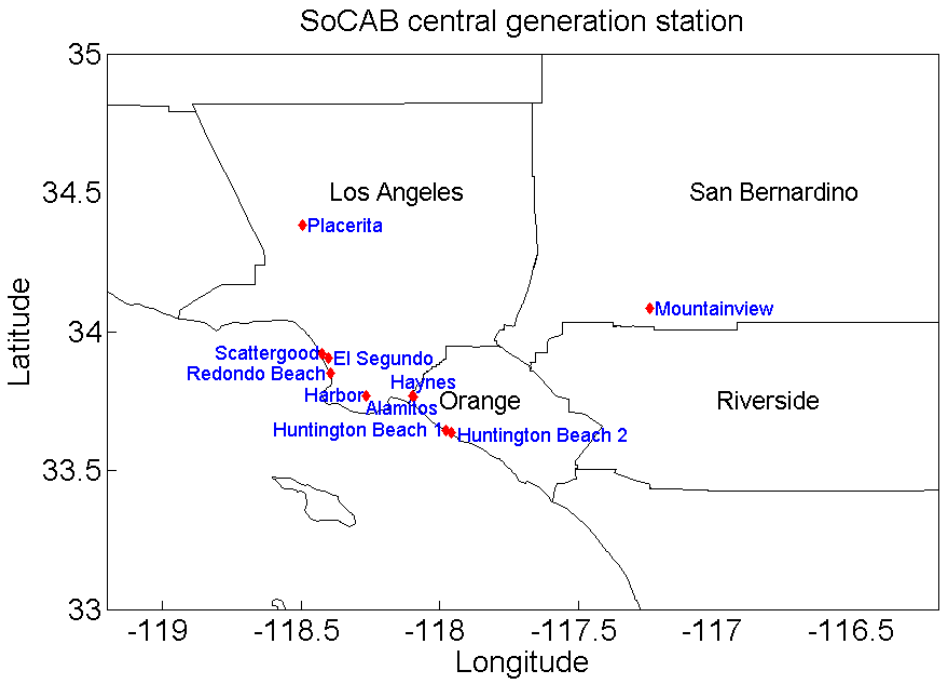


**Figure 3-6. Locations of the ten CGs in the SoCAB.**

The air quality impact of the two scenarios were compared by running AERMOD using meteorological inputs corresponding to 2007 for the 26 meteorological stations shown in Figure 3-1. The impact of a specific CG or DG was calculated by using the meteorological inputs from the nearest station. The modeling domain is divided into 5 km

by 5 km grids, and the spatially averaged annual concentration was calculated for each grid cell. Using another scale for the spatial average does not change the results qualitatively.

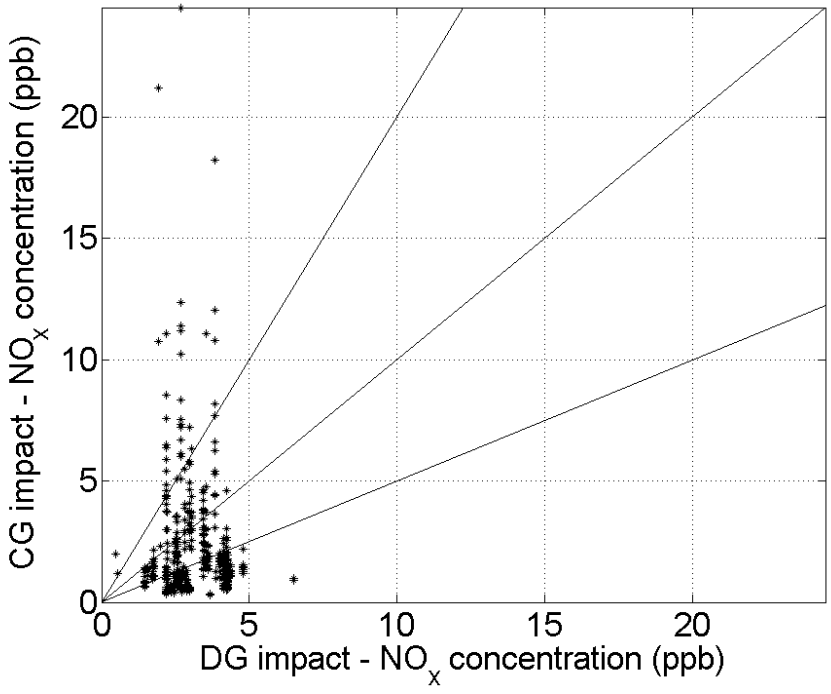


**Figure 3-7. Comparison of hourly maximum concentration for the two scenarios.**

We see from Figure 3-7 that although the averages of hourly maximum concentrations have the same magnitude, 3 ppb for the scenario in which the EHP power demand is met by CGs and 2 ppb for the scenario in which the demand is met by DGs, the CG scenario produces a peak hourly maximum concentration of about 25 ppb which is about four times higher than that of the DG scenario, 6 ppb. As expected, locations close to CG stations see larger hourly maximum concentrations when CGs rather than DGs are used

to generate power as seen in Figure 3-8. Even in the interior of the basin, the hourly maximum concentrations from the CGs and DGs are comparable because of the much higher emissions from CGs.

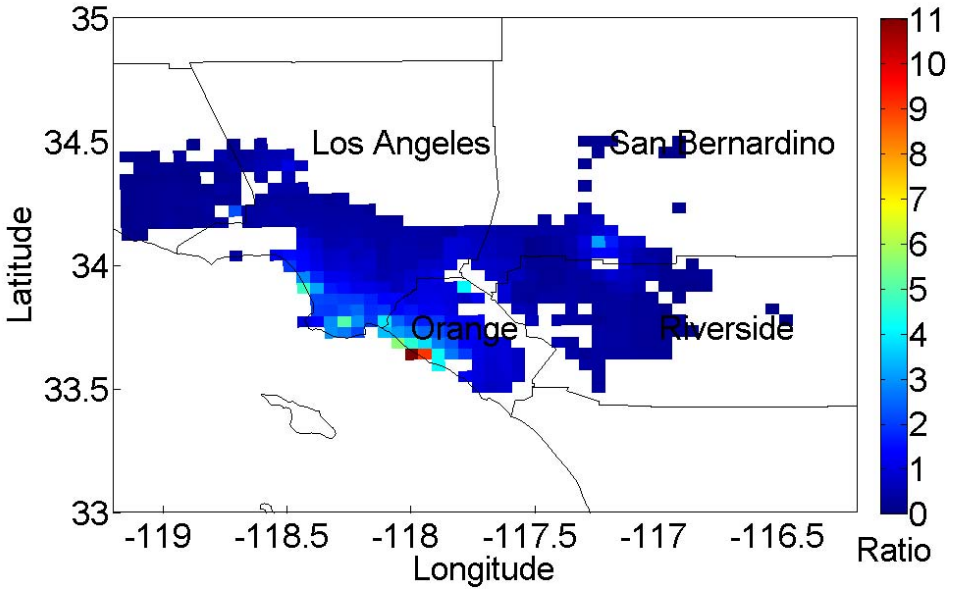


**Figure 3-8. The ratio of hourly maximum concentrations of the CG scenario to those of the DG scenario in the LA basin.**

We see from Figure 3-9 that the scenario in which all the EHP power demand is met by CGs results in lower grid averaged annual concentrations for most of the basin than the scenario in which the demand is met by DGs. For about half of the basin, the air quality impact of the CG scenario is a factor of 0.5 smaller than that of the DG scenario.

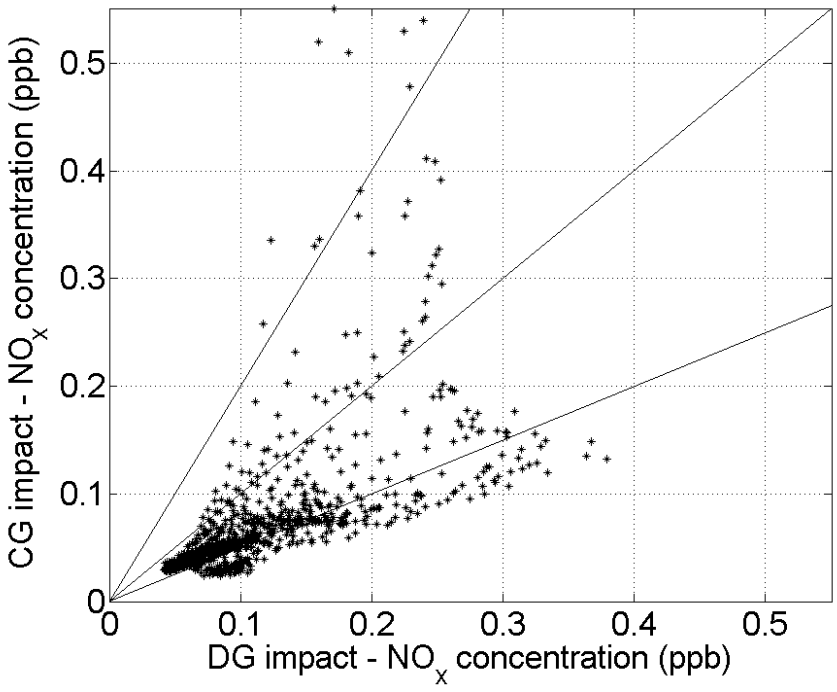


**Figure 3-9. Comparison of grid-averaged annual concentration for the two scenarios.**

As expected, locations close to CG stations see larger increases when CGs rather than DGs are used to generate power as seen in Figure 3-10. CGs have lower annually averaged impacts than DGs because they are located at the borders of the basin so that their impacts are evident only when the wind blows from the CGs into the interior of the basin. On the other hand, DGs are densely distributed in the interior of the basin to satisfy local power demands. Thus, their annually averaged impact does not depend on wind direction, and they have an opportunity to act cumulatively for all wind directions. Note that maximum concentrations do not depend on the frequency of wind direction, so that CGs still give rise to the highest annual concentrations.

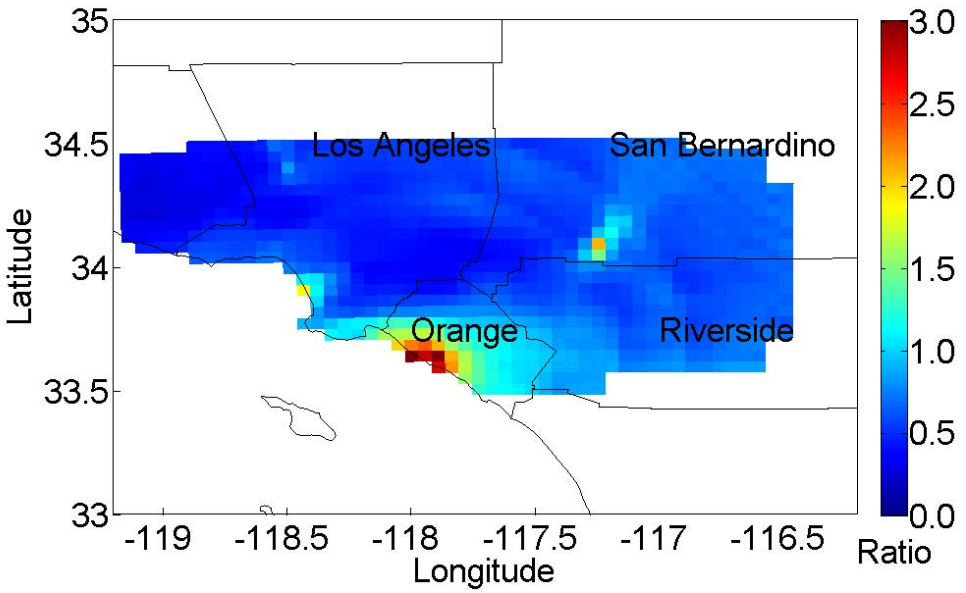


**Figure 3-10. The ratio of grid-averaged concentration of the CG scenario to that of the DG scenario.**

The marginal impacts of the additional power generation were then estimated by adding the computed annual impacts of these two scenarios to the 2007 $NO_2$ levels in the SoCAB. This assumes that all the $NO_x$ is converted into $NO_2$.

There are currently 36 active air quality monitoring stations in SoCAB (CARB, 2003). Figure 3-11 shows the 2007 $NO_2$ annual concentrations for each grid cell. The annual concentrations are associated with the data of the nearest monitoring stations, which are obtained from the SCAQMD historic database (SCAQMD, 2009b). The 2007 annual averages of $NO_2$ near the Pomona meteorological station was 31.8 ppb, which is above the annual CA state $NO_2$ standard of 30 ppb.

Note that the maximum impact of both scenarios is less than 10% of the existing $NO_2$ levels. Future DG penetration into the SoCAB will add an annual average of 0.1 ppb to

the existing level of 20 ppb in the basin assuming that the monitored values correspond to 5 km spatial averages. Expanding existing CGs will add 0.05 ppb to the existing $NO_2$ levels. The resulting $NO_2$ annual averages near the Central LA meteorological station exceed the CA standard, where the 2007 level was 29.9 ppb, just below the standard. The two scenarios show similar results, except that the DG scenario has a few more grid cells that exceed the standard than the CG scenario.

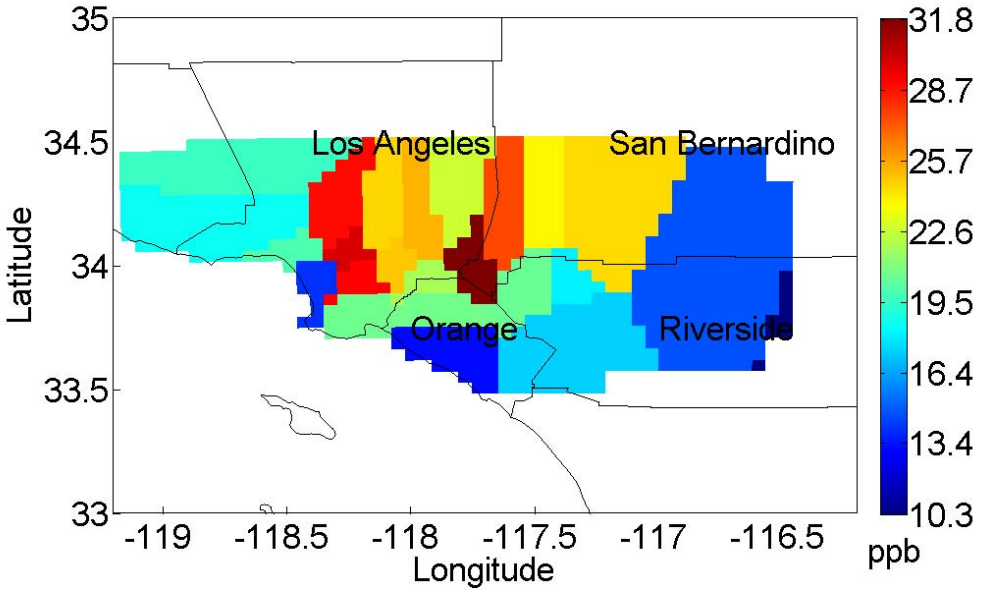


**Figure 3-11. Annually averaged $NO_2$ concentrations in the SoCAB In 2007**

### 3.5 Conclusions

We estimate the air quality impact of generating the projected increase in power demand in the South Coast Air basin by 2010 by using distributed generators. This impact is compared to that resulting from an expansion of existing CG stations to meet the increased demand. The relative impacts were calculated using AERMOD, a state-of-the-

art dispersion model developed by the USEPA. We used maximum hourly and spatially and annually averaged $NO_x$ concentrations as comparison metrics.

The main conclusions of this study are:

a) The maximum hourly $NO_x$ nominal concentrations associated with most CGs are at least a factor of two higher than those of DGs because of the much higher emissions from CGs. The maximum impact on hourly concentrations in the basin can be reduced from 25 ppb to 6.0 ppb if DGs rather than CGs are used to generate power. This result is important in view of the recently promulgated 1 hour $NO_2$ standard, 100 ppb (USEPA, 2010).

b) The grid averaged annual concentrations (long-term exposure from the DG scenario) are generally higher than those from the CG scenario over most of the basin. Over half of the basin, the annually air quality impact of the DG scenario is about a factor of two larger than that of the CG scenario. Future DG penetration into the SoCAB will add an annual average of about 0.1 ppb to the existing level of about 20 ppb in the basin while expanding existing CGs will add about 0.05 ppb to the existing level. The impact of DG penetration is likely to be smaller if their emissions are offset by the decrease in boiler emissions if waste heat from the DGs is captured.

c) The area near Central LA station will exceed the California $NO_2$ annual standard if any generating capacity is located in the area.

The secondary conclusions of this study are:

a) When the wind speeds are low, about a 1 m/s, plume rise plays a major role in determining ground-level concentrations associated with small buoyant sources such as DG stations. Maximum ground-level concentrations of primary emissions can decrease with power increase because the increase in emissions with power can be more than offset by the increase in plume rise with power.

b) Waste heat recovery is likely to increase the maximum ground-level concentrations in the vicinity of a DG, especially when the average winds are low, because of the decrease in plume rise. This conclusion is relevant to locating DGs in urban areas where wind speeds are typically low because of sheltering by buildings.

c) The concentration averaged over a distance of 50 km of the source due to both DGs and CGs is insensitive to the effective stack height. It increases with the increase of the power and the decrease of the mean wind speed. The average concentration due to most individual CGs is at least a factor of twenty higher than that due to DGs because of much higher emissions from CGs.

## 4. Impact of Distributed Generation of Electricity Relative to Other Urban Sources

### 4.1 Introduction

In chapter 3, we show that shifting electricity generation from CGs to DGs will change the $NO_x$ level in the LA basin, but the significance of this change relative to all other urban sources remains unknown. There is a need to develop methods to allow the comparison of the impact of DG relative to other background urban sources.

The air quality in an urban area is affected by a large number of sources, such as vehicles, distributed over the urban area. Thus, the contribution of sources within meters from an urban receptor might be comparable to that of sources outside the local area of interest. In principle, an air quality model can be used to estimate the contributions of all the urban sources to concentrations at a receptor. However, the large number and variety of sources in an urban area necessitates computational resources that can become impractical even with current computers, especially when it is necessary to conduct sensitivity studies over long averaging times. The current approach to this problem is to use models applicable to several scales so that sources at different distances from the area of interest can be treated with different levels of source aggregation. The concentration at a receptor has three components: a regional contribution computed from a long-range transport model with a grid spacing of the order of tens of kilometers, an urban "background" contribution from sources aggregated over kilometer sized grids, and a local contribution from models that estimate concentrations at meters from a receptor (See Brandt et al., 2003 for an example).

This chapter focuses on a model that estimates urban "background" concentrations of $NO_x$, $NO_2$, and $O_3$, averaged over a scale of the order of kilometers. In the usual numerical solution of the mass conservation equation governing concentrations, transport and chemistry are treated simultaneously or as processes that follow each other within a numerical time step. This coupling treatment is adopted in most grid models, such as CMAQ (Byun and Schere, 2006) and UCI-CIT (Carreras et al., 2004). The chemistry module in these grid models, however, occupies a large portion of computing time, and their application becomes a computational burden if concentrations are required over a year. The simple urban background model (UBM) developed by Berkowicz (2000) addresses this problem through two simplifications: a straight line steady dispersion model and chemistry based on photostationarity neglecting the role of hydrocarbons. The model presented here is intermediate between comprehensive photochemical models and the simple UBM. It treats unsteady meteorological conditions with trajectories that reflect space and time varying winds, and it reduces the computational requirements of photochemical models by separating transport and chemistry using a method described in Venkatram et al. (1998). The model is evaluated with data from measurements made in Los Angeles (CARB, 2011).

## 4.2 Methods

We suggest reducing the computational requirement of the grid model by separating transport and chemistry. The model presented in this chapter replaces the coupled processes of transport and chemistry by first performing the transport and then

performing chemistry over a time interval corresponding to the age associated with transport. The transport is based on a receptor-based Lagrangian model in which back trajectories are used to trace the history of a moving box arriving at a receptor. The chemical species emitted into the box are first transported without accounting for chemistry. However, each species is associated with an effective age in addition to concentrations. The species are then allowed to react in a box over a time corresponding to the maximum of the ages of the species that arrive at the receptor. The photochemical model used to produce ozone concentrations in this chapter is the Carbon Bond IV mechanism (Gery et al., 1985), in which the volatile organic compounds (VOC) are assumed to be a mixture typical of ambient measurements made in Los Angeles; the VOC is distributed among 8 surrogate species and one inert species.

### 4.2.1 The Lagrangian Model

The model, based on that proposed by Venkatram and Cimorelli (2007), computes the concentrations at a receptor by following the history of an air parcel that reaches a receptor of interest every hour. The history of the air parcel is traced back 24 hours through back trajectories calculated using surface winds measured at meteorological stations. To facilitate the use of the model, the meteorological inputs are taken directly from the surface input files used by AERMOD (Cimorelli et al., 2005).

The air parcel has horizontal dimensions of 5 km by 5 km, and a height that depends on the local mixed layer height. Emissions are injected into the box and mixed through its volume as the box moves over the urban area, which is described with a gridded emission

inventory of $NO_x$ and VOC. To ensure pollutants are well mixed, we carefully choose a time step which is higher than the mixing time scale given by $\sqrt{2/\pi}\, z_i/\sigma_w$. For the meteorological conditions used in the study for the SoCAB, this mixing time scale has a maximum value of about 0.9 h. Therefore, we can use a time step $\Delta t = 1\text{h}$ to trace back the history of the box for 24-hours. The concentrations are stepped from the $(i\text{-}1)^{\text{th}}$ to the $i^{\text{th}}$ time step through

$$C_i = C_{i-1} \min\left(\frac{z_{i-1}}{z_i}, 1\right) \exp(-v_d \Delta t / z_i) + \frac{\Delta m_i}{z_i} \exp(-(v_d/2)\Delta t / z_i)\,, \qquad (4\text{-}1)$$

where $z_i$ is the mixed layer height and $v_d$ is the deposition velocity. We assume that the deposition velocity of newly emitted pollutants is half of the velocity of those transported from the previous step. The minimum term on the right hand side of the equation ensures that the concentration does not increase when the mixed layer decreases during a time step.

The mass of pollutant injected per unit surface area of the air parcel is $\Delta m_i = q_i(\vec{r})\Delta t$, where $q_i(\vec{r})$ is the emission density at the location of the parcel, $\vec{r}$, and $\Delta t$ is the time step of the trajectory calculate. Figure 4-1 illustrates the described Lagrangian model.

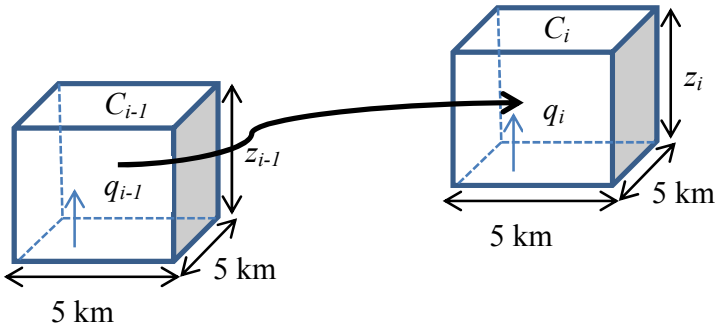


**Figure 4-1. Illustration of the Lagrangian model.**

The incremental concentration, $\Delta C_i$, during the last hour of the air parcel's path is computed with a steady state dispersion model (Venkatram and Cimorelli, 2007) that accounts for incomplete vertical mixing,

$$\Delta C_i = \sqrt{2/\pi}\ln(1 + \sigma_w R/(Uh))q_i/\sigma_w, \quad (4\text{-}2)$$

where $R$ is half of the grid length, $U$ is the mean wind speed, $\sigma_w$ is the standard deviation of the vertical velocity fluctuations, and $h$ is the initial vertical spread of surface emissions.

When the pollutant is well mixed through the boundary layer during the last time step before the parcel reaches the receptor, equation is modified,

$$\Delta C_i = \sqrt{2/\pi}\ln\left(\sqrt{2/\pi}\, z_i/h\right) q_i/\sigma_w + q_i(R - R_m)/(Uz_i), \quad (4\text{-}3)$$

where $R_m$ is a critical length scale which determines if the pollutant are well mixed.

### 4.2.2 The Species Age

The concept of species age is best illustrated by Venkatram et al. (1994, 1998). The effective age of a molecule is the time taken for the molecule to travel from source to receptor. Considering a case in which a source emits $NO_x$ and the wind speed is $u_i$, we can simply calculate the age of the molecules at a distance $x_i$ from the source as $x_i/u_i$. This simple case can be generalized to more complex wind flows by formulating a conservation equation for species age. The formulation is best understood by examining each of the processes that determine the aging of molecules enclosed within a control volume. The underlying concept is that an average age can be associated for each of the species in a grid volume.

The differential equation for the age, $A$, of a species can be formulated by considering the following: 1) The age of material in a control volume increases with time if nothing is emitted into the box; 2) The average age decreases when new material is emitted into the volume; 3) Transport of material into and out of the volume changes the age.

Consider a box in which the mass per unit surface area of a certain species changes from $m(t)$ to $m(t+\Delta t)$ and the age changes from $A(t)$ to $A(t+\Delta t)$ in the time interval $\Delta t$. The age $A(t+\Delta t)$ is determined by the ages of material that flow into the box and aging of the material that is already in the box. Then the conservation of age for a box with dimensions, $\Delta x_i$, along the coordinate direction, $i$, can be written as

$$A(t+\Delta t)m(t+\Delta t) = m(t)(A(t)+\Delta t) - \frac{\Delta(u_i m A)}{\Delta x_i}\Delta t \,. \tag{4-4}$$

The first term on the right-hand side of the eq. (4-4) refers to the aging of the material in the box during the interval $\Delta t$, and the second term corresponds to the contribution of the material transported into the box at a rate $u_i m$ by the instantaneous velocity, $u_i$. If we define $\varphi \equiv Am$, the differential corresponding to eq. (4-4) can be written as

$$\frac{D\varphi}{Dt} = \frac{\partial\varphi}{\partial t} + \frac{\partial(u_i\varphi)}{\partial x_i} = m \,. \tag{4-5}$$

where the left-hand side is the Lagrangian derivative defined along the trajectory of the box moving with a velocity $u_i$.

If there are no emissions along the trajectory, the mass density of the species will remain constant, and we can integrate equation (4-5) to obtain $\varphi = mt$, which leads to the conclusion that the species age is equal to the travel time along the box trajectory, $A(t)=t$.

Considera casein which the mass density increases linearly with time as a result of emissions, $m(t) = \alpha t$, where $\alpha$ is a constant. Substituting this mass into equation (4-5) and integrating yields the result that the age is one-half of the travel time, $A(t) = t/2$. This result is consistent with the idea that new emissions reduce the average age of the species associated with the moving box. Thus, the ages can be computed from the $(i\text{-}1)^{th}$ to the $i^{th}$ time step through a numerical version of equation (4-5)

$$\varphi(i) - \varphi(i-1) = \Delta t\,(m_i + m_{i-1})/2 = m_i \Delta t - \Delta m_i \cdot (\Delta t/2), \qquad (4\text{-}6)$$

which can be rearranged as

$$A_i = A_{i-1}(1 - \Delta m_i/m_i) + \Delta t(1 - \Delta m_i/(2m_i)). \qquad (4\text{-}7)$$

In the absence of fresh emissions, that is $\Delta m_i = 0$, we obtain the expected result: $A_i = A_{i-1} + \Delta t$. Note that fresh emissions always decrease the effective age of the species within the parcel, that is, $A_i < A_{i-1} + \Delta t$.

Then, the chemical transformation of this species is estimated by reacting it with other species in a box with initial concentrations corresponding to those in the absence of chemistry. The time period for chemical calculations is specified by the end time corresponding to the time of interest and a start time, which is the end time minus the species age. The chemical calculation is performed over the maximum of the ages of the species in the air parcel. The chemistry accounts for the variation of photolysis rates with time of day.

### 4.3 Model Evaluation

The model is applied to estimating $NO_x$, $NO_2$, and $O_3$ concentrations in the South Coast Air Basin (SoCAB) of Los Angeles, depicted in Figure 4-2. The upper panel of the figure shows the $NO_x$ emissions developed by Samuelsen et al. (2005) for the SoCAB, which correspond to a total $NO_x$ emission rate of 413 tons/day. The lower panel shows the assumed diurnal variation of $NO_x$ emissions, which roughly corresponds to traffic volume. The background ozone is taken to be 30 ppb. In view of the uncertainty in VOC emissions, we do not calculate VOC concentrations in the air parcel, but assume that the VOC concentrations are a constant multiple of the computed $NO_x$ concentrations, which is taken to be 6 in our case. We then add a background VOC concentration of 20 ppbC. Such empirical adjustments to the VOC concentrations are not unusual even in comprehensive grid based modeling.

The model was run with surface meteorological data corresponding to 2007, measured at 26 meteorological stations operated by the South Coast Air Quality Management District (See Figure 3-1, SCAQMD, 2009). Model estimates are compared with $NO_x$ concentrations measured at 21 monitoring stations operated by California Air Resources Board (CARB, 2011), which are numbered in the upper panel of Figure 4-2.

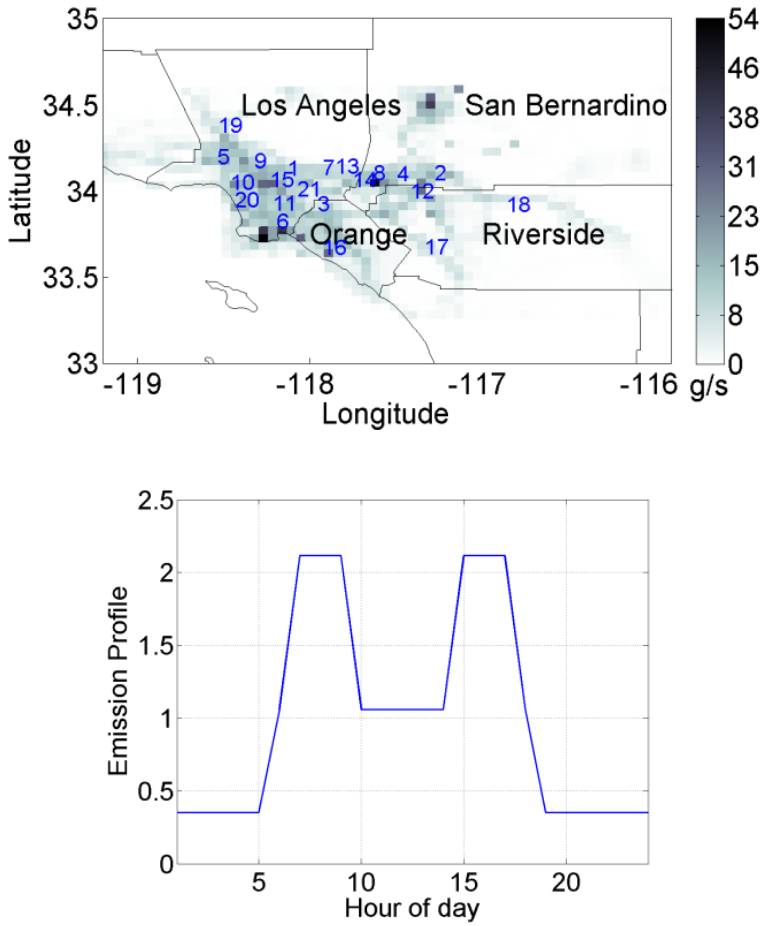


**Figure 4-2. Gridded $NO_x$ emissions and monitoring stations located in the South Coast Air Basin, Los Angeles. The right panel shows the assumed temporal profile of $NO_x$ emissions.**

Model performance is described in terms of the statistics of the ratio $C_p/C_o$ (Venkatram et al. 2005). This method is based on the assumption that the observations, $C_o$, are lognormally distributed about the predicted estimates, $C_p$, so that:

$$\ln(C_o) = \ln(C_p) - \varepsilon. \tag{4-8}$$

Therefore $\varepsilon$ can be taken as the residual:

$$\varepsilon = \ln(C_p/C_o) \tag{4-9}$$

and it can be used to quantify model performance. The bias in the model estimate is characterized by $m_g$, the geometric mean of the ratio:

$$m_g = \exp(\bar{\varepsilon}), \tag{4-10}$$

where ¯ represents mean. The spread of observations about a model estimate is quantified by using geometric standard deviation, $s_g$:

$$s_g = \exp\big(\sigma(\varepsilon)\big), \tag{4-11}$$

where $\sigma$ represents standard deviation. Then, if the observed values are lognormally distributed about the model estimates, the 95% confidence interval of the ratio of the observed to the estimated value is approximately given by the interval $m_g s_g^{1.96}$ to $m_g s_g^{-1.96}$. By doing so, a bias greater than unity implies overprediction, and a bias less than unity implies underprediction. The coefficient of determination, $r^2$, refers to the variation of $\ln(C_o)$ explained by the model; it is the square of the correlation coefficient between $\ln(C_o)$ and $\ln(C_p)$. The fraction of the ratios, $C_p/C_o$, which lies in the range 0.5 - 2 is denoted by *Fac2*.

Figure 4-3 shows typical 24-hour back-trajectories of air parcels at two monitoring sites on July 31, 2007. The back trajectory is calculated using the available meteorological station in the SoCAB (Figure 3-1). One site is near the Fontana meteorological station. The south-western mean winds originate from the Pacific Ocean, cross the shoreline, blow over Orange County and arrive at the monitoring site. The other site is located near the La Habra meteorological station. The winds originate again from the Pacific Ocean, cross the shoreline and arrive at the monitoring station.

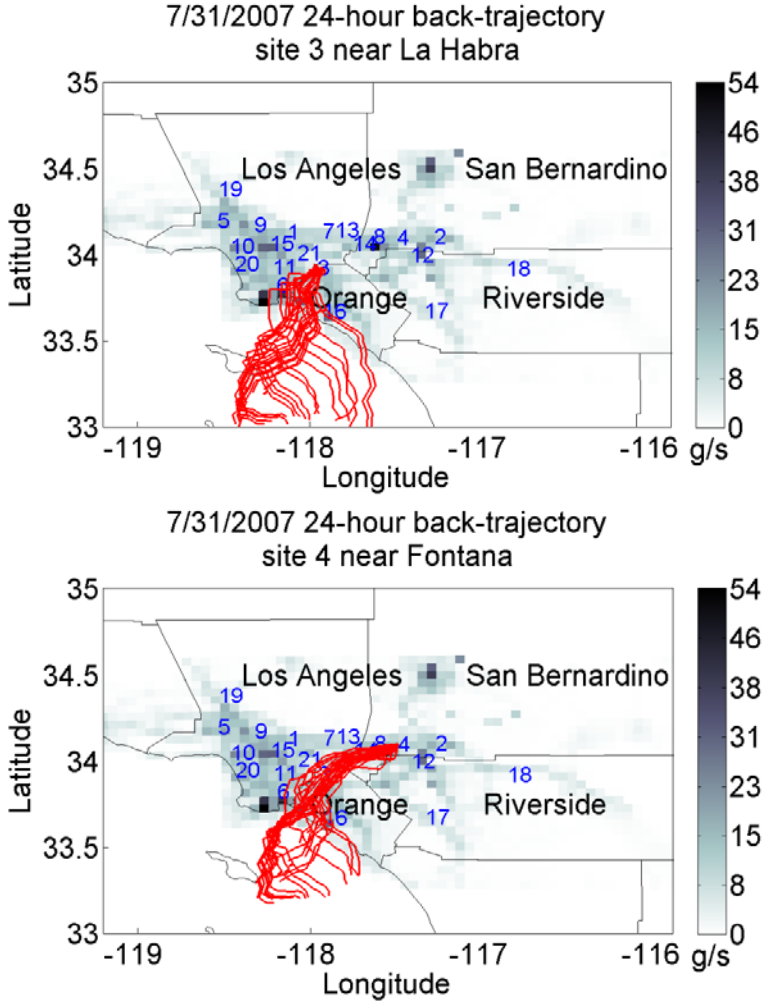


**Figure 4-3. 24-hour back-trajectories of air parcels at two monitoring sites on July 31, 2007**

The performance of the model is illustrated by considering the same two sites. The upper two panels of Figure 4-4 show that the modeled $NO_x$ and $NO_2$ concentrations, averaged over a month, are well correlated with the corresponding observations. However, the model overestimates the $NO_2$ during the fall months at the Fontana site and underestimates $NO_x$ during the winter months at the La Habra site the as seen in Figure 4-4.

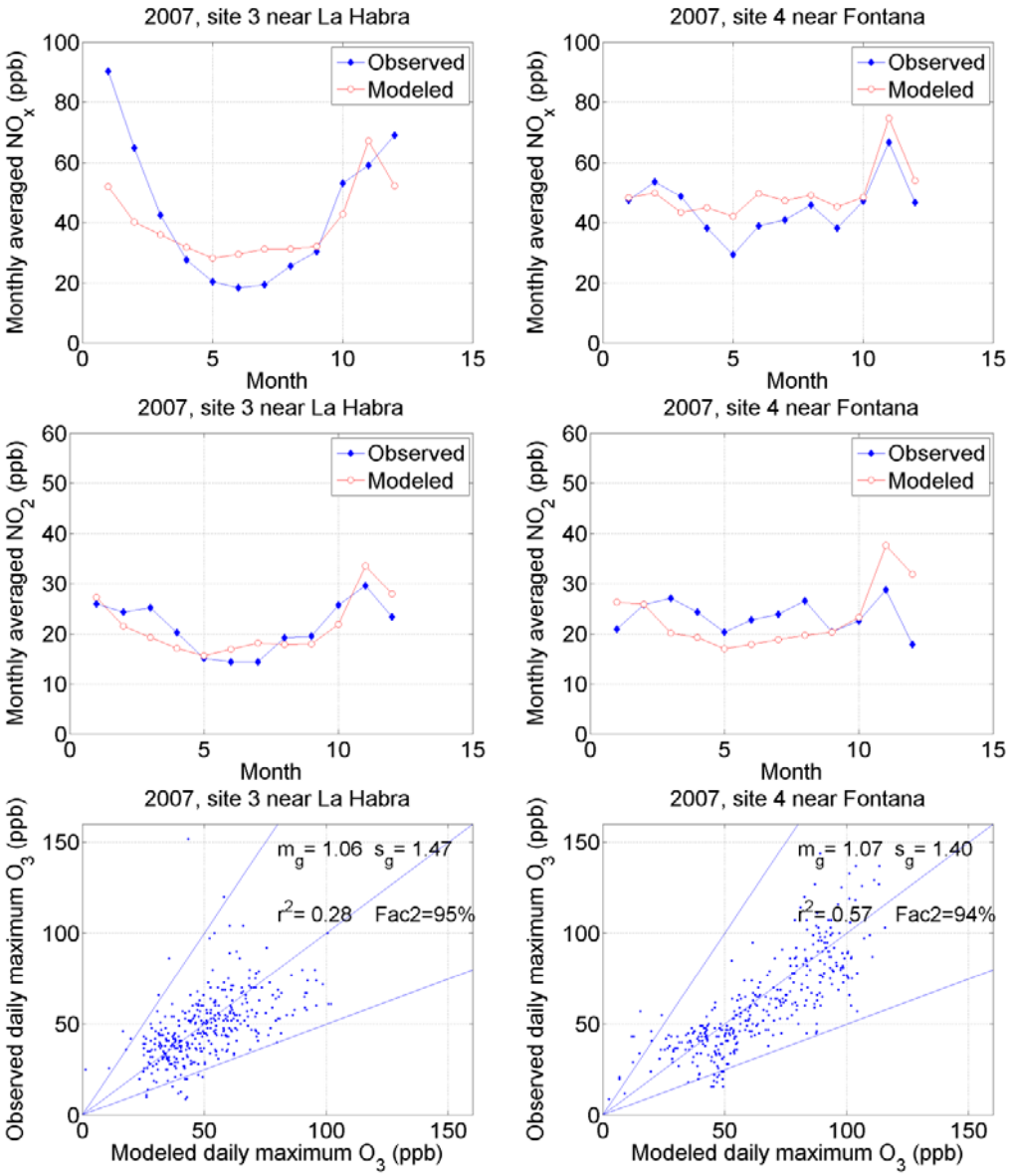


**Figure 4-4. Monthly averaged $NO_x$, $NO_2$, and daily maximum ozone concentrations compared with observations at two sites in the SoCAB**

The lower panels of Figure 4-4 compare the modeled and observed maximum daily ozone concentrations at these stations. Although the scatter is not small, the model shows little bias as indicated by $m_g$ values close to unity. The 95% confidence intervals, $s_g^2$

(Qian et al., 2010), for the ratio of observed and estimated $NO_x$ concentrations of both sites are below 2.2. Over 90% estimations are within a factor of two. 57% observations monitored from the Fontana meteorological station can be explained by the model, but that value for the La Habra meteorological station is only 27%.

The upper two panels of Figure 4-5 shows that the model predicts averaged daily variations of $NO_x$ and $NO_2$ that are similar to those of observations. However, the model performance varies with sites. This might be related to the uncertainty in estimating the mixed layer height. It could also be associated with the assumed temporal profile of $NO_x$ emissions. The lower panels of Figure 4-5 show that the model captures the averaged daytime variation of $O_3$, but it underestimates it during the early morning.

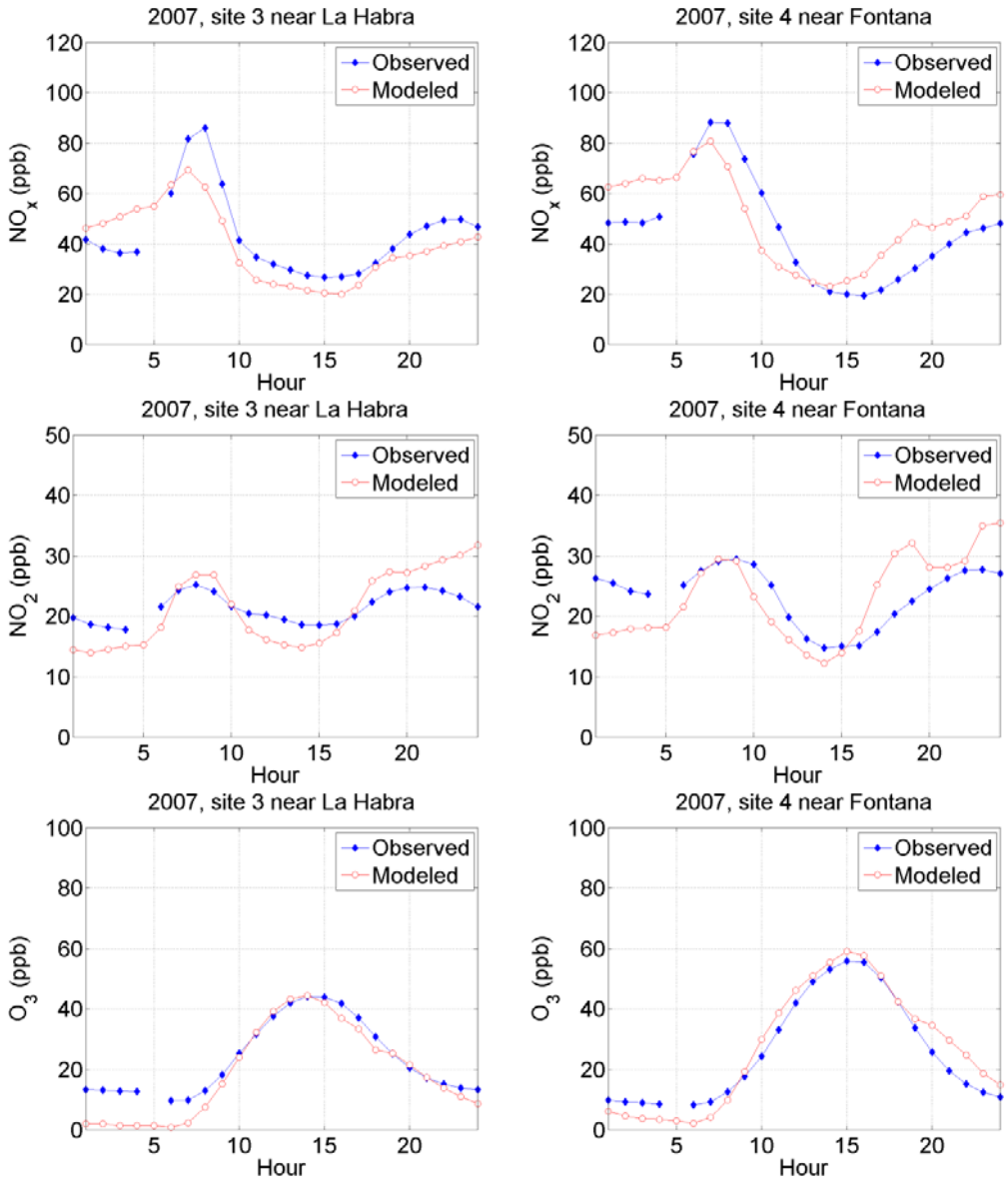


**Figure 4-5. Averaged daily variations of $NO_x$, $NO_2$ and $O_3$ compared with observations at two sites in the SoCAB.**

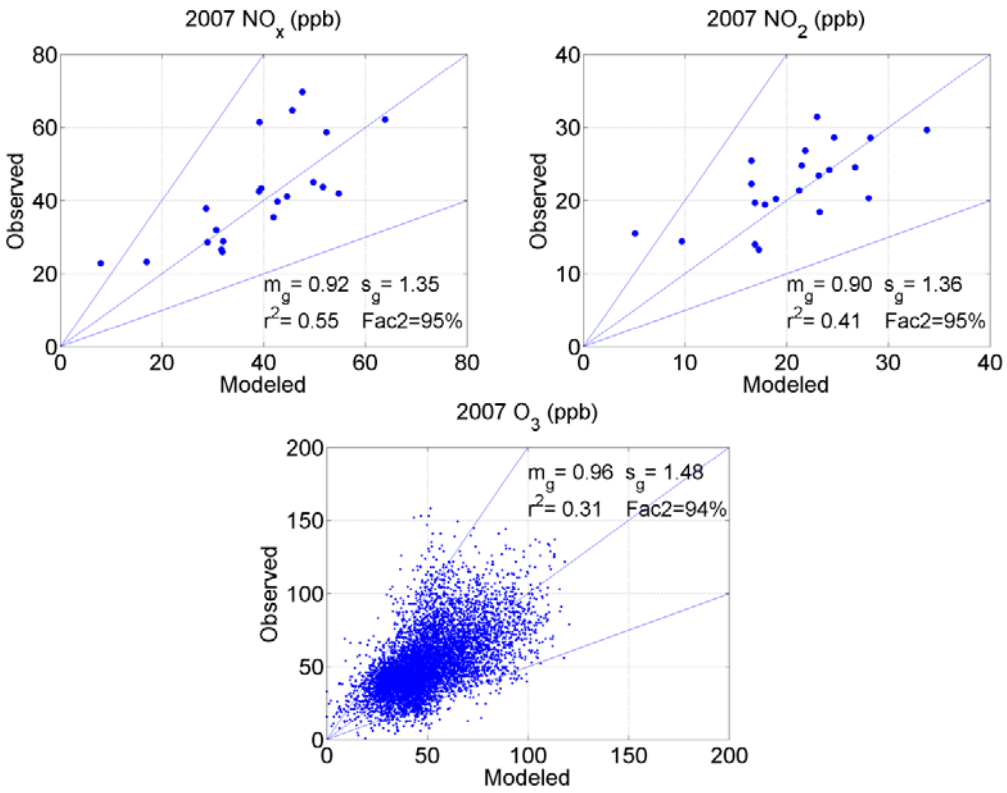


**Figure 4-6. Annually averaged $NO_x$ and $NO_2$ concentrations and daily maximum $O_3$ concentrations of all 21 sites in the SoCAB compared with observations.**

The upper two panels of Figure 4-6 shows the overall model performance in explaining annually averaged $NO_x$ and $NO_2$ concentrations of 21 monitoring sites in SoCAB. The model underestimates $NO_x$ and $NO_2$ by 10%, but it can explain over 40% observations. 95% of the model estimates are within a factor of two of the observations. The 95% confidence interval for the ratios of observed to estimated $NO_x$ and $NO_2$ concentrations is 1.8. The only site which the model underestimates both $NO_x$ and $NO_2$ more than a factor of two is site 18, Banning Airport monitoring station. This could be related with the mountains standing in both south and north sides of the site. The simple two-dimensional trajectory model presented in this chapter does not take terrain into consideration.

The lower panel of Figure 4-6 shows the overall model performance in explaining daily maximum $O_3$ concentrations of all 21 sites. The bias is 4%, although it only explains 30% of observations. More than 90% of model estimates are within a factor of two of the observations. The 95% confidence interval for the ratio of observed to estimated $O_3$ concentrations is 2.2.

### 4.4 The Air Quality Impact of a DG Deployment Relative to the Background Sources in the SoCAB

Section 3.4.2 compared the relative impacts of a DG and CG deployment in the SoCAB. This section compares the predicted air quality of the DG deployment relative to the sources (refer to as 'background sources') described in section 4.3. We use $NO_x$ as a surrogate for primary pollutants. Future work may use concentrations of $NO_x$, $NO_2$, $O_3$ and VOC predicted in section 4.3 as backgrounds for estimating concentrations of secondary pollutants due to DG deployment. Methods for combining estimates from regional transport models with those from local dispersion models have been proposed by Hess and Cope (1989), Isakov et al. (2007), and Stein et al. (2007).

The upper panel of Figure 4-7 shows that the maximum hourly $NO_x$ concentrations of the background sources at 21 sites are at least 30 times higher than those of the DG, and the minimum hourly impacts of the background sources are just slightly lower than the maximum hourly impacts of the DG deployment at most sites, because the emission rate of background sources, 413 tons/day, is much higher than the one of the DG deployment, 4.4 tons /day if DGs meet the California $NO_x$ emission standard for a new generation device, 32 g/MWh. The lower panel of Figure 4-6 shows that the annually averaged $NO_x$

concentrations of the background sources are at least 100 times higher than those of the DG.

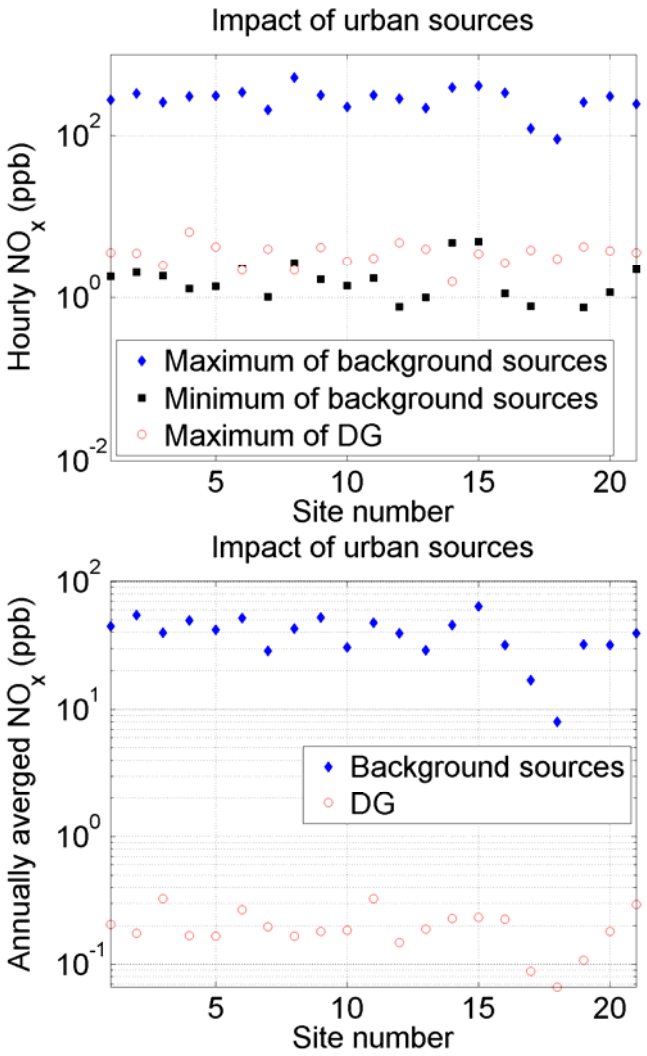


**Figure 4-7. Comparing $NO_x$ concentration of the DG deployment and the background sources. Upper panel: Hourly concentration; lower panel: annually averaged concentration.**

## 4.5 Conclusions

We have formulated a simple Lagrangian model that can be used to estimate background concentrations of $NO_x$, $NO_2$, and $O_3$ in an urban area. The model can provide hourly concentrations of these species over time periods of a year, which is required in exposure studies. It can be used to estimate the air quality impact of DG relative to other sources in an urban area. The model achieves its computational efficiency by separating transport and chemistry using the concept of species age. Evaluation with measurements made in SoCAB during 2007, indicates that the model can provides adequate descriptions of the spatial and temporal behavior of $NO_x$ and $NO_2$. Model estimates of maximum hourly ozone concentrations are unbiased relative to observations but the 95% confidence interval ($s_g^2$) of the ratios of observed to estimated concentrations is over a factor of two.

## 5. Conclusions

The research reported in this dissertation is motivated by the need to model the air quality impact of Distributed Generation (DG) of electricity on $NO_x$ and $NO_2$ relative to other sources of $NO_x$. The dispersion of DG type sources is first understood through a tracer field experiment, which also facilitates the evaluation of AERMOD's applicability to low level buoyant sources in urban areas. Then AERMOD is used to estimate the impact of DG on air quality relative to Central generation (CG) of electricity that DG is designed to replace. The last part of the thesis describes a Lagrangian model that can be used to compare the impact on air quality all other urban sources relative to that of DG.

The first part of this thesis described a tracer study conducted in July 2008 in the vicinity of a 650 kW gas fired power plant located in Palm Springs, CA. AERMOD (Cimorelli et al., 2005) was evaluated with the tracer data. The major conclusions from this part of my research are:

a) Concentrations observed during the nighttime experiments are generally higher than those measured during the daytime experiments. They fall off less rapidly with distance than during the daytime.
b) AERMOD provides an adequate description of concentrations associated with a buoyant release from DG during the daytime when turbulence is controlled by convection induced by solar heating.
c) The inclusion of meandering in AERMOD is important in explaining the occurrence of upwind concentrations during low wind speeds.

d) AERMOD underestimates concentrations during the night when turbulence is generated by wind shear. It predicts a decrease in concentrations with distance that is much more rapid than the relatively flat observed decrease.

e) A modification to AERMOD to account for different rates of plume growth in the upper and lower part of the nighttime boundary layer leads to a significant improvement in model performance.

f) AERMET, AERMOD's meteorological processor, provides a poor description of the nighttime boundary layer. Local measurements or better estimation of meteorology are needed by AERMOD to prevent severe underestimation in predicting concentrations.

The second part of this dissertation examines the air quality impact of using DG to satisfy future growth in power demand in the South Coast Air Basin of Los Angeles (SoCAB), relative to the impact when the demand is met by expanding current CG capacity. The impact of decreasing boiler emissions by capturing the waste heat from DGs is not examined. The air quality impacts of these two alternate scenarios are quantified in terms of hourly maximum ground-level and annually-averaged primary $NO_x$ concentrations, which are estimated using AERMOD. The study focuses on the impact of primary emissions at source-receptor distances of tens of kilometers. The main conclusions of this study are:

a) The maximum hourly $NO_x$ nominal concentrations associated with most CGs are at least a factor of two higher than those of DGs because of the much higher emissions from CGs. The shift to DGs has the potential for decreasing maximum

hourly impacts of power generation in the vicinity of the DGs. The maximum hourly concentration is reduced from 25 ppb to 6 ppb if DGs rather than CGs are used to generate power.

b) The grid averaged annual concentrations (long-term exposure) from the DG scenario are generally higher than those from the CG scenario over most of the basin. Future DG penetration will add an annual average of 0.1 ppb to the current basin average, 20 ppb, while expanding existing CGs will add 0.05 ppb.

c) The area near Central LA station will exceed the California $NO_2$ annual standard if any generating capacity is located in the area.

d) When the wind speeds are low, about a 1 m/s, plume rise plays a major role in determining ground-level concentrations associated with small buoyant sources such as DG stations. Maximum ground-level concentrations of primary emissions can decrease with power increase because the increase in emissions with power can be more than offset by the increase in plume rise with power.

e) Waste heat recovery is likely to increase the maximum ground-level concentrations in the vicinity of a DG, especially when the average winds are low, because of the decrease in plume rise. This conclusion is relevant to locating DGs in urban areas where wind speeds are typically low because of sheltering by buildings.

f) The concentration averaged over a distance of 50 km of the source due to both DGs and CGs is insensitive to the effective stack height. It increases with the increase of the power and the decrease of the mean wind speed. The average

concentration due to most individual CGs is at least a factor of twenty higher than that due to DGs because of much higher emissions from CGs.

The third part of my thesis focused on formulating a model to estimate concentrations of $NO_2$, $NO_x$, and $O_3$ averaged over a spatial scale of the order of a kilometer in a domain extending over tens of kilometers. The model can be used to estimate hourly concentrations of these species over time periods of years. It achieves the required computational efficiency by separating transport and chemistry using the concept of species age. Evaluation with data measured at 21 stations distributed over the Los Angeles air basin indicates that the model provides an adequate description of the spatial and temporal variation of the concentrations of $NO_2$ and $NO_x$. Estimates of maximum hourly $O_3$ concentrations show little bias compared to observations, but the scatter is not small.

## 6. References


Allwine, K.J., Shinn, J.H., Streit, G.E., Clawson, K.L., Brown, M., 2002. Overview of URBAN 2000: a multiscale field study of dispersion through an urban environment. Bulletin of the American Meteorological Society, 83, 521–536.

Allison, J.E., Lents, J., 2002. Encouraging distributed generation of power that improves air quality: can we have our cake and eat it too? Energy Policy, 30(9), 737-752.

Barad, M.L., 1958a. Project Prairie Grass, A field program in diffusion volume I. Geophysics Research Directorate, Air Force Cambridge Research Center, Air Research and Development Command, United States Air Force, Bedford, Massachusetts.

Barad, M.L., 1958b. Project Prairie Grass, A field program in diffusion volume II. Geophysics Research Directorate, Air Force Cambridge Research Center, Air Research and Development Command, United States Air Force, Bedford, Massachusetts.

Berkowicz, R., 2000: A Simple Model for Urban Background Pollution. Environmental Monitoring and Assessment 65, 259-267.

Brandt, J., Christensen, J.H., Frohn, L.M., Berkowicz, R., 2003: Air pollution forecasting from regional to urban street scale--implementation and validation for two cities in Denmark. Physics and Chemistry of the Earth, Parts A/B/C 28, 335-344.

Briggs, G.A., 1969. Optimum Formulas for Buoyant Plume Rise. Philosophical Transactions of the Royal Society of London. Series A, Mathematical and Physical Sciences 265, 197-203.

Briggs, G.A., 1973: Diffusion estimation for small emissions. In ERL, ARL USAEC Report ATDL-106. U.S. Atomic Energy Commission, Oak Ridge, Tennessee.

Britter, R.E., Hanna, S.R., 2003. Flow and dispersion in urban aereas. Annual Review of Fluid Mechanics, 35, 469-496.

Byun, D.W., Ching, J.K.S., 1999. Science algorithms of the EPA models-3 Community Multiscale Air Quality (CMAQ) modeling system. EPA/600/R-99/030. U.S. Environmental Protection Agency, Research Triangle Park, NC.

Byun, D., Schere, K.L., 2006. Review of the Governing Equations, Computational Algorithms, and Other Components of the Models-3 Community Multiscale Air Quality (CMAQ) Modeling System. Applied Mechanics Reviews 59, 51-77.

CARB, 2003. Quality assurance air monitoring site information. California Environmental Protection Agency, Air Resources Board, Sacramento, CA <http://www.arb.ca.gov/qaweb/sitelist_create.php>.

CARB, 2011: California air quality data for the years 1980-2009. Air Resources Board, Sacramento, CA < http://www.arb.ca.gov/aqd/aqdcd/aqdcddld.htm>.

Carreras, M., Medrano, M., Samuelsen, G.S., Brouwer, J., Rodriguez, M.A., Dabdub, D., 2004. Urban Air quality impacts of distributed generation, Proceedings of ASME Turbo Expo, 2004, Vienna, Austria.

CEC, 2006. California distributed energy resources guide. California Energy Commission, Sacramento, CA <http://www.energy.ca.gov/distgen/index.html>.

CEC, 2009. Database of California power plants (Excel spreadsheet of plants greater than 0.1 megawatt). California Energy Commission, Sacramento, CA <http://energyalmanac.ca.gov/powerplants/POWER_PLANTS.XLS>.

Cheng, H., Castro, I. P., 2002. Near wall flow over urban-like roughness. Boundary-Layer Meteorol. 104, 229–259.

Cimorelli, A.J., Perry, S.G., Venkatram, A., Weil, J.C., Paine, R., Wilson, R.B., Lee, R.F., Peters, W.D., Brode, R.W., 2005. AERMOD: A dispersion model for industrial source applications. Part I: general model formulation and boundary layer characterization. Journal of Applied Meteorology, 44(5), 682-693.

Csanady, G.T., Hilst, G.R., Bowne, N.E., 1967. The diffusion from a cross-wind line source at Fort Wayne, Indiana. Unpublished Report, Travelers Research Center, Hartford, CT.

Eckman, R.M., 1994. Re-examination of empirically derived formulas for horizontal diffusion from surface sources. Atmospheric Environment, 28, 265-272.

Foken, T., 2006. 50 Years of the Monin–Obukhov Similarity Theory. Boundary-Layer Meteorology 119, 431-447.

Gery, M.W., Whitten, G.Z., Killus, J.P., Dodge, M.C., 1989. A photochemical kinetis mechanism for urban and regional scale computer modeling. J. Geophys. Res., 94.

Grimmond, C.S.B., Oke, T.R., 2002. Turbulent heat fluxes in urban areas: observations and a local-scale urban meteorological parameterization scheme (LUMPS). Journal of Applied Meteorology 41, 792-810.

Gryning, S.E., Batchvarova, E., 2005. Advances in urban dispersion modelling. NATO advanced research workshop: Advances in air pollution modelling for environmental security, Borovetz (BG), 8–12, May 2004

Gryning, S., Lyck, E., 1984. Atmospheric dispersion from elevated sources in an urban area: comparison between tracer experiments and model calculations. Journal of Climate and Applied Meteorology, 23, 651–660.

Hanna, S., Britter, R., Franzese, P., 2003. A baseline dispersion model evaluated with Salt Lake City and Los Angeles tracer data. Atmospheric Environment, 37, 5062–5069.

Heath, G.A., Hoats, A.S., Nazaroff, W.W., 2003. Air pollutant exposure associated with distributed electricity generation. Project report for California Air Resources Board, contract No. 01-341.

Heath, G.A., Granvold, P.W., Hoats, A.S., Nazaroff, W.W., 2006. Intake fraction assessment of the air pollutant exposure implications of a shift toward distributed electricity generation. Atmospheric Environment, 40(37), 7164-7177.

Heath, G.A., Nazaroff, W.W., 2007. Intake-to-delivered-energy ratios for central station and distributed electricity generation in California. Atmospheric Environment, 41(39), 9159-9172.

Iannucci, J., Horgan, S., Eyer, J., Cibulka, L., 2000. Air pollution emission impacts associated with economic market potential of distributed generation in California. California Air Resources Board Research Division.

Jing, Q., Pankratz, D., Princevac, M., Venkatram, A., 2009. Modeling dispersion of buoyant releases in an urban area. 11th Conference on Atmospheric Chemistry in the 89th American Meteorological Society Annual Meeting, Phoenix, AZ.

McElroy, J.L., Pooler, F., 1968. The St. Louis dispersion study volume II-analysis. National Air Pollution Control Administration, Pub. No. AP-53, US DHEW Arlington, 50p.

Medrano, M., Brouwer, J., Samuelsen, G.S., Carreras, M., Dabdub, D., 2003. Urban Air quality impacts of distributed generation, Proceedings of ASME Turbo Expo, 2003, Atlanta, Georgia, USA.

Monin, A.S., Obukhov, A.M., 1954. Basic laws of turbulent mixing in the ground layer of the atmosphere. Akad. Nauk. SSSR, Geofiz. Inst. Trudy 151, 163-187.

Oke, T.R., 2003. Boundary layer climates, 2nd ed. ed. Routledge., London, New York.

Perry, S.G., Cimorelli, A.J., Paine, R.J., Brode, R.W., Weil, J.C., Venkatram, A., Wilson, R.B., Lee, R.F., Peters, W.D., 2005. AERMOD: A dispersion model for industrial source applications. Part II: Model performance against 17 field study databases. Journal of Applied Meteorology, 44(5), 694-708.

Princevac, M., Venkatram, A., 2007. Estimating micrometeorological inputs for modeling dispersion in urban areas during stable conditions. Atmospheric Environment 41, 5345-5356.

Rodriguez, M.A., Carreras-Sospedra, M., Medrano, M., Brouwer, J., Samuelsen, G.S., Dabdub, D., 2006. Air quality impacts of distributed power generation in the South Coast Air Basin of California 1: Scenario development and modeling analysis. Atmospheric Environment, 40, 5508-5521.

Qian, W., Princevac, M., Venkatram, A., 2010. Using temperature fluctuation measurements to estimate meteorological inputs for modelling dispersion during convective conditions in urban areas. Boundary-Layer Meteorology, 135, 269-289.

Qian, W., 2010. Investigation of dispersion and micrometeorology under spatially inhomogeneous conditions. University of California, Riverside, United States.

Qian, W., Venkatram, A., 2011. Performance of steady-state dispersion models under low wind-speed conditions. Boundary-Layer Meteorology, 138, 475-491.

Raupach, M. R., Antonia, R. A., and Rajagopalan, S., 1991, Rough-wall turbulent Boundary Layers. Appl. Mech. Rev. 44, 1–25.

Rotach, M. W., 1993a. Turbulence close to a rough urban surface part I: reynolds stress. Boundary-Layer Meteorol. 65, 1–28.

Rotach M.W., 1993b. Turbulence close to a rough urban surface, part II: sariances and gradients. Boundary-Layer Meteorol. 66, 75–92.

Rotach, M.W., Vogt, R., Bernhofer, C., Batchvarova, E., Christen, A., Clappier, A., Feddersen, B., Gryning, S.E., Martucci, G., Mayer, H., Mitev, V., Oke, T.R., Parlow, E., Richner, H., Roth, M., Roulet, Y.A., Ruffieux, D., Salmond, J.A., Schatzmann, M., Voogt, J.A., 2004. BUBBLE – an urban boundary layer meteorology project. Theoretical and Applied Climatology, 81, 231-261.

Roth M., 2000. Review of atmospheric turbulence over cities. Quarterly Journal of the Royal Meteorological Society 126: 941-990.

Samuelsen, S., Dabdub, D., Brouwer, J., Medrano, M., Rodriguez, M., Carreras-Sosedra, M., 2005. Air quality impacts of distributed generation. California Energy Commission, PIER Energy-Related Environmental Research, CEC-500-2005-069-F.

SCAQMD, 2009a. 26 sites with AERMOD-ready meteorological data. South Coast Air Quality Management District, Diamond Bar, CA <http://www.aqmd.gov/smog/metdata/AERMOD.html>.

SCAQMD, 2009b. Historical data by year – 2007 Air quality data tables. South Coast Air Quality Management District, Diamond Bar, CA < http://www.aqmd.gov/smog/AQSCR2007/aq07card.pdf >.

Sagendorf J.F., Dickson C.R., 1974. Diffusion under low wind speed inversion conditions. NOAA Technical Memorandum ERL ARL-52, 89pp.

Salmond, J.A. and McKendry, I.G., 2005. Turbulence in the very stable nocturnal boundary layer: Implications for air pollution, Progress in Physical Geography. Vol. 29, No. 2, p171-188

Smith, D.B., 1967. Tracer study in an urban valley (Johnstown, Pennsylvania). M. S. Thesis in Meteorology, Pennsylvania State University, University Park, PA.

Stull, R.B., 1988. An introduction to boundary layer meteorology. Kluwer Academic Publishers, Dordrecht; Boston.

USEPA, 1995. User's guide for the Industry Source Complex (ISC3) dispersion model, volume II: description of model algorithms. U.S. Environmental Protection Agency Office of Air Quality Planning and Standards Emissions, Monitoring, and Analysis Division Research Triangle Park, North Carolina. EPA-454/B-95-003b.

USEPA, 2003. AERMOD:Latest feature and evaluation. Office of Air Quality Planning and Standards, Emissions and Monitoring and Analysis Division, Research Triangle Park, NC.

USEPA, 2007. Criteria air pollutants inventory – Final 2002 NEI Version 3. US Environmental Protection Agency, Washington, DC <ftp://ftp.epa.gov/EmisInventory/2002finalnei/2002_final_v3_2007_summaries/point/allneicap_annual_11302007.zip> .

USEPA, 2008. The emission and generation resource integrated database (eGrid2007 Version 1.1). US Environmental Protection Agency, Washington, DC <http://www.epa.gov/cleanenergy/documents/egridzips/eGRID2007_Version1-1.zip>.

USEPA, 2010. National ambient air quality standards. US Environmental Protection Agency, Washington, DC <http://www.epa.gov/air/criteria.html>.

Venkatram, A., 1980. Dispersion from an elevated source in a convective boundary layer. Atmospheric Environment, 14, 1-10.

Venkatram, A., 1982. A semi-empirical method to compute concentrations associated with surface releases in the stable boundary layer. Atmospheric Environment, 16, 245-248.

Venkatram, A., Strimaitis, D., Dicristofaro, D., 1984. A semiempirical model to estimate vertical dispersion of elevated releases in the stable boundary layer. Atmospheric Environment, 18, 923-928.

Venkatram, A., Paine, R., 1985. A model to estimate dispersion of elevated releases into a shear-dominated boundary layer. Atmospheric Environment, 19, 1797-1805.

Venkatram, A., Karamchandani, P., Pai, P., Goldstein, R., 1994: The development and application of a simplified ozone modeling system (SOMS). Atmospheric Environment, 28, 3665-3678.

Venkatram, A., Du, S., Hariharan, R., Carter, W., Goldstein, R., 1998: The concept of species age in photochemical modeling. Atmospheric Environment, 32, 3403-3413.

Venkatram, A., 1999. Applying a framework for evaluating the performance of air quality models. Proceedings of the Sixth International Conference on Harmonisation within Atmospheric Dispersion Modeling for Regulatory Applications, Rouen, France, 11-14 October, 1999.

Venkatram, A., 2004. The role of meteorological inputs in estimating dispersion from surface releases. Atmospheric Environment, 38, 2439-2446.

Venkatram, A., Isakov, V., Pankratz, D., Heumann, J., Yuan, J., 2004a. The analysis of data from an urban dispersion experiment. Atmospheric Environment, 38, 3647-3659.

Venkatram, A., Isakov, V., Yuan, J., Pankratz, D., 2004b. Modeling dispersion at distances of meters from urban sources. Atmospheric Environment, 38, 4633-4641.

Venkatram, A., 2005. An examination of the urban dispersion curves derived from the St. Louis dispersion study. Atmospheric Environment, 39, 3813-3822.

Venkatram, A., Cimorelli, A.J., 2007: On the role of nighttime meteorology in modeling dispersion of near surface emissions in urban area. Atmospheric Environment, 41, 692-704.

Venkatram, A., Princevac, M., 2008. Using measurements in urban areas to estimate turbulent velocities for modeling dispersion. Atmospheric Environment 42, 3833-3841.

Venkatram, A., Lee, S., Jing, Q., Qian, W., 2010. Evaluation of the near source air quality impact of distributed generation. California Energy Commission, PIER Energy-Related Environmental Research Program, MAQ-07-03.